

# The dynamics of adaptive neuronal networks: influence of topology on synchronisation

Simon Aertssen, s181603

## *Supervisors*

Erik Martens  
Poul Hjorth

February 1<sup>st</sup> 2021

# Contents

Abstract . . . . .	II
<b>1 Nomenclature</b>	<b>III</b>
<b>2 Introduction</b>	<b>4</b>
<b>3 The Theta Neuron Model</b>	<b>5</b>
3.1 Canonical neuron models . . . . .	5
3.2 Theta Neuron model description . . . . .	5
3.3 Solutions for static currents . . . . .	6
3.4 Numerical solutions . . . . .	7
3.5 Frequency response . . . . .	7
3.6 Phase response . . . . .	8
<b>4 Network Topologies</b>	<b>9</b>
4.1 Representations and properties . . . . .	9
4.2 Fixed-degree networks . . . . .	9
4.3 Random / Erdős-Rényi networks . . . . .	9
4.4 Scale-free networks . . . . .	10
4.5 Networks of theta neurons . . . . .	11
<b>5 Mean Field Reductions</b>	<b>12</b>
5.1 The Ott-Antonsen manifold . . . . .	12
5.2 Simplifications for fixed-degree networks . . . . .	13
5.3 Implications and challenges of the <i>MFR</i> . . . . .	14
<b>6 <i>Investigation:</i> Mean Field Reductions for undirected graphs</b>	<b>15</b>
6.1 Directed graphs as permutations . . . . .	15
6.2 Building the adjacency matrix . . . . .	16
6.3 Initial conditions: analytical versus numerical approaches . . . . .	16
6.4 Final conditions . . . . .	19
6.5 Commutativity of complex vectors . . . . .	19
6.6 Fixpoint iteration . . . . .	20
6.7 A Newton-Raphson iteration for all fixpoints . . . . .	20
6.8 Fixed-degree networks as a baseline . . . . .	21
6.9 Results for arbitrary network topologies . . . . .	21
<b>7 Hebbian Learning and Synaptic Plasticity</b>	<b>25</b>
7.1 Spike-timing dependant plasticity . . . . .	25
7.2 Formulations of <i>STDP</i> as a model . . . . .	26
7.2.1 The Kempter method . . . . .	26
7.2.2 The Song method . . . . .	27
7.3 Synaptic scaling . . . . .	28
7.4 Intrinsic plasticity . . . . .	29
<b>8 <i>Investigation:</i> Emerging Network Topologies</b>	<b>30</b>
8.1 Conditions of the network . . . . .	30
8.2 Tuning hyperparameters for $W_K$ . . . . .	30

8.3	Results of using <i>STDP</i>	31
8.4	Results of using <i>STDP + IP</i>	31
<b>9</b>	<b>Conclusion and Discussion</b>	<b>35</b>
<b>10</b>	<b>References</b>	<b>36</b>
<b>A</b>	<b>Appendix</b>	<b>38</b>
A.1	Transformation to the QIF model	38
A.2	Solutions to the QIF model	38
A.2.1	Solving for $I < 0$	38
A.2.2	Solving for $I = 0$	38
A.2.3	Solving for $I > 0$	38
A.3	Frequency response of the neuron models	39
A.4	Newton-Raphson root iteration	39
A.5	Jacobian of the Ott-Antonsen manifold	39

## Abstract

The synchronisation of networks of oscillators, network topology and network plasticity can only be understood using a holistic approach, and each domain is investigated in relation to the other. The Theta neuron model is analysed to understand feedback mechanisms between the electrical current and the phase response. Different network topologies are then described in terms of their degree distribution. Networks of Theta neurons are studied using the synchronisation of the mean-field. Inspired by the process of synaptic plasticity, learning rules are then established to observe emergent network topologies.

# 1 Nomenclature

$i, e$ (or $\exp$ )	Imaginary unit. Euler's number.
$n$	Network node
$N$	Network degree. The number of neurons in the network.
$A_{ij}$	Adjacency matrix. Models which neuron $i$ is connected to neuron $j$ and vice-versa.
$\langle k \rangle$	Average node degree in the network.
$\deg(n) = \mathbf{k}$	Degree of node $n$ , as a vector of the in- and out-degree of a single node as $(k^{\text{in}}, k^{\text{out}})$ .
$\mathbf{k}^{\text{in}}, \mathbf{k}^{\text{out}}$	Node degree vector of all in- and out degrees of the network.
$M_k$	Number of unique node degrees in the network.
$P(k), P(\mathbf{k})$	Univariate and bivariate network degree distribution.
$k_{\min}, k_{\max}$	Smallest and largest degree in a network.
$\gamma$	Degree exponent of a scale-free network.
$p$	Probability threshold of forming a link in random networks.
$c$	Assortativity of the network.
$\theta_i(t)$	Phase variable function of the theta model (of neuron $i$ ).
$\mathcal{P}_n(\theta)$	Pulse-shaped synaptic coupling function.
$\kappa$	Macroscopic coupling strength.
$\eta_i, I_i(t)$	Excitability threshold and input current (of neuron $i$ ).
$g(\eta \mathbf{k})$	Excitability threshold distribution with mean $\eta_0(\mathbf{k})$ and width $\sigma(\mathbf{k})$ .
$Z(t)$	Kuramoto order parameter function.
$z(\mathbf{k}, t)$	Synchronisation dynamics function for nodes with degree $\mathbf{k}$ .
$\bar{Z}(t)$	Mean field order parameter function for arbitrary networks.
$S_i^{\text{in}}(t), S_i^{\text{out}}(t)$	Spike trains received and emitted by neuron $i$ as a sum of delta functions in time.
$K_{ij}$	Synaptic connectivity matrix. Strength of the connections between neurons $i$ and $j$ .
$\Delta t_{ij}$	Time difference between spikes of neurons $i$ and $j$ .
$W(t)$	Learning window. Models the correlation between synaptic strength and spike times.
$\phi(t)$	IP learning function. Models correlation between excitability strength and spike times.
$\mathbb{T}$	Set of angles in $[-\pi, \pi[$ .
$\mathbb{K}$	Set of unique degrees in a network, support of $P$ .
$\mathbb{R}, \mathbb{C}$	Set of real and complex numbers.
$\mathbb{C}_{\circ}$	Set in the complex unit circle so that $\mathbb{C}_{\circ} = \{z \in \mathbb{C} :  z  \leq 1\}$ .
$F(v), F^{-1}(v)$	Random permutation and inverse permutation of the elements of a vector $v$ .

## 2 Introduction

In 2013, the European Union launched one of the largest funded scientific project ever. With the Human Brain Project [1], scientists and researchers aimed to reconstruct the human brain through supercomputer-based models and to advance neuroscience, medicine, and computing. Across the globe different fields of science are drawing inspiration from the human brain.

One such approach is to model the behaviour of biological neurons and to quantify the information processes in the brain from stimuli from the senses or from electrical and chemical processes in the body. A given neuron receives hundreds of impulses in the form of neurotransmitters from its neighbours, almost exclusively on its dendrites and cell body. These stimuli add up to an excitatory or inhibitory influence on the electrical membrane potential of the neuron, so that the potential spikes when excitation is higher than an internal threshold. This explosion of electrical activity is called the *action potential* [2]. At the neurons synapse, the action potential is converted into a chemical signal again, in the form of a neurotransmitter release, and the neuron joins the interneuronal communication [8]. Most neurons in the central nervous system use either the excitatory neurotransmitter glutamate (AMPA or NMDA) or the inhibitory neurotransmitter GABA [9, 10]. We will speak of the presynaptic neuron as the neuron that sends a signal and of the postsynaptic neuron as the neuron that receives a signal.

The neuron dynamics are largely captured by this spiking behaviour, on which most efforts of finding a description have been concentrated. In 1952, Hodgkin and Huxley formulated a mathematical model for the action potentials in neurons, using a set of nonlinear differential equations that approximates the electrical characteristics of the neuron elements. In 1963 the authors were awarded the Nobel Prize in Physiology or Medicine [3] for their work.

As the human brain contains more than 100 billion neurons [4] it is unfeasible to study complex models at this scale, setting aside the complexity of the Hodgkin-Huxley model. The topology of neuronal networks displays traits of small-worldness, wiring optimisation, and heterogeneous degree distributions [5], for which it is difficult to pin down one type of network architecture. Through the mean-field reduction (*MFR*) proposed in [6] one can reduce a large network of indistinguishable neurons to a low-dimensional dynamical system, described by the attraction of a mean-field variable to a reduced manifold. In this work we will study the *MFR* of different types of networks of pulse-coupled Theta neurons using the generalisations found in [7].

Neurons have the ability to adjust the intensity of their response to in- and outbound signals depending on the neurons activity in a process called *synaptic plasticity*. We can observe how neurons release a different quantity of neurotransmitters, or relocate the neurotransmitter receptors. The average intensity of the response is referred to as the *synaptic strength*. Plastic changes to the brain structure are believed to be the foundation of learning and the memory. One can quantify and model these changes to the network topology using Hebb's postulate on the correlation of neuron activity in the network [11]. Changes to the network topology are easily modeled as changes to the synaptic strength.

The work presented here is thus two-fold: we study the dynamics of pulse-coupled networks *on* networks, and the dynamics *of* such networks when they evolve over time.

### 3 The Theta Neuron Model

#### 3.1 Canonical neuron models

A number of neuron model families have been identified, and often there exists a continuous change of variables from models of the same family into a *canonical* model that can represent the whole family [12]. As the transformation is not required to be invertible, we can study the universal neurocomputational properties of the family in a low dimensional model. It was Hodgkin [13] who classified neurons into two types based on their excitability, upon experimenting with the electrical stimulation of cells. Class 1 models begin to spike at an arbitrarily slow rate, and the spiking frequency increases when the applied current is increased. Class 2 models spike as soon as their internal threshold is exceeded and the spiking frequency stays relatively constant within a certain frequency band [12].

#### 3.2 Theta Neuron model description

In [14], a Class 1 canonical phase model was proposed:

$$\dot{\theta} = (1 - \cos \theta) + (1 + \cos \theta) \cdot I \quad \theta \in \mathbb{T} \quad (1)$$

with  $I$  a bifurcation parameter on the supplied current. We can visualise the dynamics on the unit circle, like in Figure 1. The neuron produces a spike when  $\theta$  surpasses  $\pi$ , upon which  $\theta \leftarrow -\pi$ .

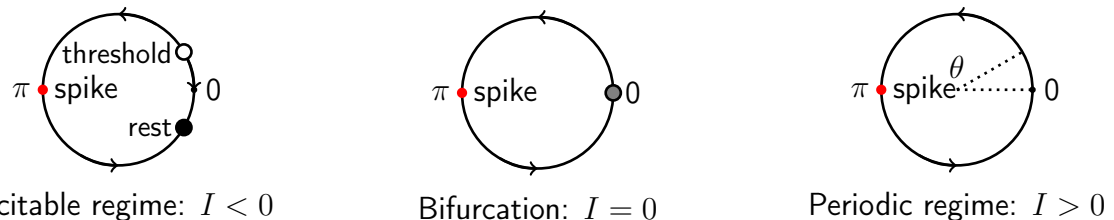


Figure 1: SNIC bifurcation of the theta neuron model. A spike occurs when  $\theta = \pi$ . For  $I < 0$ , the neuron is in a rest state but *excitable* and we observe one stable and one unstable equilibrium point. For  $I > 0$ ,  $\dot{\theta} > 0$  so that  $\theta$  moves continuously around the circle and we can observe *periodic* sustained spiking. The saddle-node bifurcation occurs at  $I = 0$ , so that  $\theta$  will spike when it is larger than 0.

We can recognise the features of the class 1 model in Figure 2. This makes (1) the normal form of the *saddle-node-on-invariant-circle* (SNIC) bifurcation [15], as it collapses  $\mathbb{R}$  to  $\mathbb{T}$ .

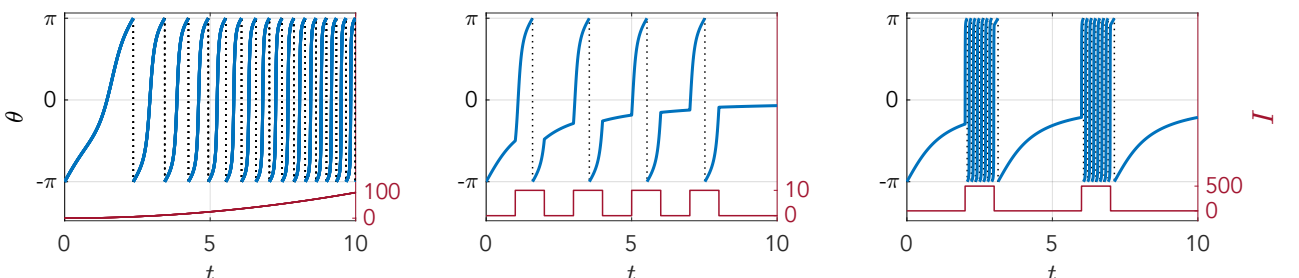


Figure 2: Properties of the theta neuron model, with solutions of (1) in blue, spikes marked in dotted lines, and the current  $I$  in red. Left: the spike frequency of  $\theta$  increases as  $I$  is increased over time, which is the distinguishing feature of class 1 canonical models. Middle: spikes occur within a finite time period when  $I > 0$  and within infinite time when  $I = 0$ . Right: when  $I$  is large, the neuron *bursts*.

Equilibria only exist for the *excitable* regime  $I < 0$ :

$$\begin{aligned} \dot{\theta} &= 1 - \cos \theta + I + I \cdot \cos \theta = (I + 1) + (I - 1) \cdot \cos \theta \\ \theta_{1,2}^* &= \pm \arccos \left( \frac{I+1}{1-I} \right) + 2\pi n \end{aligned}$$

We can find the stability of the equilibria through:

$$\frac{d}{d\theta}((1 - \cos \theta) + (1 + \cos \theta) \cdot I) = \sin \theta - \sin \theta \cdot I = (1 - I) \cdot \sin \theta$$

In the equilibria this yields:

$$\frac{d}{d\theta}(\theta_{1,2}^*) = \pm(1 - I) \cdot \sqrt{1 - \left(\frac{I+1}{1-I}\right)^2} = \pm(1 - I) \cdot \frac{2\sqrt{-I}}{1-I} = \pm 2\sqrt{-I}$$

This yields an unstable equilibrium point for  $\theta_1^*$  and a stable for  $\theta_2^*$ . This means that as  $\theta$  gets perturbed above  $\theta_1^*$ , a spike occurs and  $\theta$  converges to  $\theta_2^*$ . This is demonstrated in Figure 3.

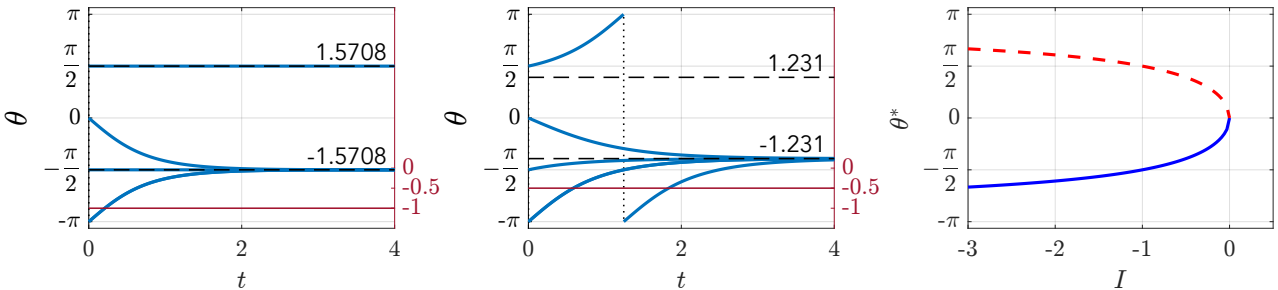


Figure 3: Equilibria  $\theta^*$  for different values of  $I$ . Left:  $I = -1$  yields  $\theta_{1,2}^* = \pm \frac{\pi}{2}$ , one of the simulations is started exactly on the unstable equilibrium. Middle:  $I = -0.5$ . Right: bifurcation diagram of the SNIC bifurcation, with the stable equilibria in blue, and the unstable in red.

### 3.3 Solutions for static currents

Gaining insight into (1) is hard, due to the difficulty of finding an analytical solution. However, it has been noted that there exists a simple transformation which yields (see A.1):

$$V \equiv \tan\left(\frac{\theta}{2}\right) \quad (2)$$

$$\dot{V} = V^2 + I \quad (3)$$

This model is called the *Quadratic Integrate and Fire model* (QIF). (3) models the membrane potential of a neuron, which spikes to  $= \infty$  when the neuron spikes and is reset at  $-\infty$ . The transformation (2) is continuous between spikes, so insights from a solution for  $V$  can be transformed directly. The equilibria of the QIF model are simply  $\pm\sqrt{-I}$  (as  $I < 0$ ) so that we can express  $\theta_{1,2}^* = 2 \cdot \arctan(\pm\sqrt{-I})$ , from [16].

The solution for the excitable regime  $I < 0$  is :

$$V(t) = \frac{2\sqrt{-I}}{1 - e^{2t\sqrt{-I}}} - \sqrt{-I} \quad (4)$$

The solution at the bifurcation  $I = 0$  is :

$$V(t) = \frac{-1}{t} \quad (5)$$

The solution for the periodic regime  $I > 0$  is :

$$V(t) = -\sqrt{I} \cdot \cot(t\sqrt{I}) \quad (6)$$

These equations assume that at  $t = 0$  a spike has occurred. The steps required to find (4)-(6) are described in A.2. Solutions for  $\theta$  are found by taking the inverse of the transformation (2).

If the QIF model is so much simpler, then why bother using the Theta model? Simulating the QIF model requires an artificial reset threshold, because we cannot expect a computer to represent infinity easily. Finite thresholds make the analytical solutions more difficult and convoluted. By using the Theta model the dynamics remain smooth and bounded on  $\mathbb{T}$ .

### 3.4 Numerical solutions

When  $I$  is not static, we need to revert to numerical solutions. For this work, a fixed-step 4-stage Runge-Kutta method (Dormand-Prince 45) was implemented to numerically solve all differential equations. A fixed-step algorithm makes it possible to finely tune the large memory demand of the systems presented in this work.

### 3.5 Frequency response

As we already saw in Figure 2, an increasing current increases the spiking frequency. We can compute this relationship by measuring how long it takes for  $V$  to reach a spike: we solve (6) for  $t$  at  $V(t) = +\infty$  in A.3. This yields the oscillation period  $T = \frac{\pi}{\sqrt{I}}$  which we can see in Figure 4. We know that when  $\theta > \theta_1^*$  a spike occurs in the excitable regime, or in any case in the periodic regime. But the time that it takes to reach the spike can be arbitrarily long, depending on how close we are over  $\theta_1^*$ . So, spikes will occur, but after a delay that is dependant on the stimulus. Explicitly, if we perturb  $\theta(0) = \theta_1^* + \varepsilon$  we obtain from [16]:

$$T_{\text{spike}} = \frac{-\tanh^{-1}\left(1 + \frac{\varepsilon}{\sqrt{I}}\right)}{\sqrt{I}}$$

The delay to the spike blows up as  $\varepsilon \rightarrow 0$  so that spikes may occur after a very large delay.

In most of our future work,  $I$  will not be a static current. We ask ourselves: how sensitively does  $T$  depend on  $I$  when  $I$  is perturbed? We can measure this as a *relative* perturbation using  $dI/I$  and  $dT/T$  [2] :

$$\left| \frac{dT}{dI} \frac{I}{T} \right| = \left| \frac{dT/T}{dI/I} \right| = \left| -\frac{\pi}{2} \left( \frac{1}{\sqrt{I}} \right)^3 \frac{I}{T} \right| = \left| \frac{\pi}{2} \left( \frac{T}{\pi} \right)^3 \frac{I}{T} \right| = \frac{1}{2} \left| \left( \frac{T}{\pi} \right)^2 \left( \frac{\pi}{T} \right)^2 \right| = \frac{1}{2}$$

Hence, a 1% change in  $I$  will result in a 0.5 % change in the period.

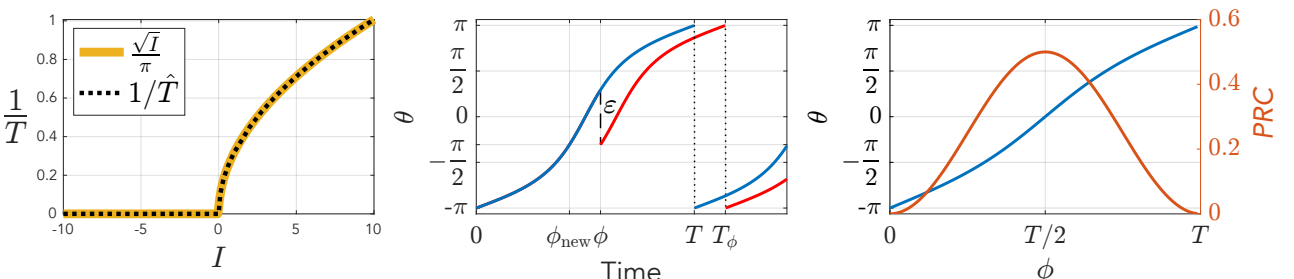


Figure 4: Response of the theta model to bifurcations on the frequency and the phase. Left: Frequency response of the theta model, experimentally verified. For  $I \leq 0$  the spike period is infinite, which is why we see the solutions to (1) approach  $\theta = 0$  for  $I = 0$  in Figure 2. Middle: a bifurcation  $\varepsilon < 0$  at time  $\phi$  perturbs  $\theta(t)$  (in blue) which results in a delayed spike (trajectory in red). Right: The PRC, (8) in red, with a solution for  $\theta$  (in blue), to show when the model is the most susceptible to bifurcations.

### 3.6 Phase response

Perturbations on the period can also be understood from the perspective of the phase. Changes to the phase  $\theta$  can delay or advance the event of a spike, and in general this depends on exactly when the stimulus occurs. The phase response curve (*PRC*) gives us exactly that relation [16, 17]. Let us define  $\phi \in [0, T[$ , which represents the time since the last event of a spike. When we add a small bifurcation  $\varepsilon$  to  $\theta$  at time  $\phi$ , a spike will occur at  $T_\phi$ , and we have that  $\theta(\phi_{\text{new}}) = \theta(\phi) + \varepsilon$ . The time to the new spike is  $T_\phi = T + (\phi - \phi_{\text{new}})$ . The *PRC* can then be defined as:

$$PRC(\phi) = T_\phi - T \quad (7)$$

This process has been visualised in Figure 4, after [17]. For infinitesimally small perturbations to the phase, we can find the *PRC* as the *adjoint* of the solution, [16], as:

$$PRC(\phi) = \frac{1}{dV(\phi)/d\phi} = \frac{1}{2\sqrt{I}} \left( 1 - \cos\left(\frac{2\pi}{T}\phi\right) \right) \quad (8)$$

We can use  $\phi \in [0, T[$  and  $\theta \in \mathbb{T}$  to see that (8) can be expressed as:

$$PRC(\theta) = \frac{1}{2\sqrt{I}} (1 + \cos \theta) \quad (9)$$

which is the magnitude with which  $I$  excites the model (1), [18]. Analysis of the *PRC* thus allows us to study how the bifurcation of  $\theta$  with magnitude  $I$  occurs.

The *PRC* is always positive, which indicates that a positive bifurcation will advance the time of the spike, and vice versa. This has also been reported as a distinguishing feature of Class 1 models [18].

## 4 Network Topologies

Networks consists of *nodes* connected by *links*. They arise in any context where objects are *related* to each other. In this section, we will look at the notation that is needed to represent networks, and properties of different network topologies.

### 4.1 Representations and properties

We represent a finite network through the adjacency matrix  $A$ : if there exists a relation from node  $j$  to node  $i$  we set  $A_{ij} = 1$ , and 0 otherwise. This means that  $A_{ij}$  can be *undirected* (symmetric) or *directed*. If we think of the relations between guests at a party, then the social network is directed, as people might not know each other mutually. However, the network of people having shaken hands is symmetric. Self-links are an edge-case that depends on the context, as one generally does not shake hands with himself.

The *degree*  $\mathbf{k}$  of a node  $n$  is a two-vector of the number of links coming in to and going out of the node,  $(k^{\text{in}}, k^{\text{out}})$ . From  $A_{ij}$  we can compute the in- and out-degree vectors, which show how many links a node has coming in and out:

$$\mathbf{k}_i^{\text{in}} = \sum_{j=1}^N A_{ij} \quad \mathbf{k}_j^{\text{out}} = \sum_{i=1}^N A_{ij} \quad \deg(n_j) = \mathbf{k}_j = (\mathbf{k}_j^{\text{in}}, \mathbf{k}_j^{\text{out}}) \in \mathbb{K} \subset \mathbb{N} \quad (10)$$

The average degree of the network is then:

$$\langle k \rangle = \frac{1}{N} \sum_{i,j=1}^N A_{ij} = \frac{1}{N} \sum_{i=1}^N \mathbf{k}_i^{\text{in}} = \frac{1}{N} \sum_{j=1}^N \mathbf{k}_j^{\text{out}} \quad (11)$$

The distribution of  $\mathbf{k}^{\text{in}}$  and  $\mathbf{k}^{\text{out}}$  is the most defining property of the network:

$$(\mathbf{k}^{\text{in}}, \mathbf{k}^{\text{out}}) \sim P(\deg(n) = \mathbf{k}) \quad (12)$$

The support of  $P$  is the set of unique degrees  $\mathbb{K}$  with cardinality  $M_k$ . As we do not allow multilinks, the largest number of links a node can make is  $N$ .  $\mathbb{K}$  is thus in principle always defined on the interval  $[0, N]$ . For symmetric networks,  $\mathbf{k}^{\text{in}} = \mathbf{k}^{\text{out}}$ , so that  $P$  is really a univariate distribution. In this case, much of the coming analysis is heavily simplified, so we will start with univariate distributions.

### 4.2 Fixed-degree networks

A network consists of nodes, connected by links. The most simple network is one where all the nodes are connected, and so all nodes have a degree of  $N$ . In general, we can make networks where all nodes have the same degree,  $\langle k \rangle$ :

$$P(k) = \begin{cases} \langle k \rangle & \text{if } k = \langle k \rangle \\ 0 & \text{otherwise} \end{cases} \quad \mathbb{K} = \{\langle k \rangle\} \quad (13)$$

We will refer to these networks as *fixed-degree* networks. When  $\langle k \rangle = N$ , all nodes are self-coupled and connected to all other nodes in the network, so we speak of a *fully connected* network.

### 4.3 Random / Erdös-Rényi networks

In 1959 Erdös and Rényi published their work on random graphs [19], where links are established if a random uniformly distributed number is higher than a threshold  $p$ . The degrees follow a binomial distribution:

$$P(k) = \binom{N-1}{k} p^k (1-p)^{N-1-k} \quad (14)$$

with a mean  $\mu = p(N - 1)$  and standard deviation  $\sigma = \mu(1 - p)$ . For networks where  $\langle k \rangle \ll N$ , the network can be well approximated by a Poisson distribution:

$$P(k) = e^{-\langle k \rangle} \frac{\langle k \rangle^k}{k!} \quad (15)$$

with a mean  $\mu = \langle k \rangle$  and standard deviation  $\sigma = \sqrt{\langle k \rangle}$ . Both (14) and (15) describe similar quantities, but the latter is used more often due to its analytical simplicity [20].

Even though (15) is theoretically defined over the entirety of  $\mathbb{N}$ , in practice, the probability of observing degrees not close to  $\langle k \rangle$  quickly drops to zero. For large random networks, we can define  $\mathbb{K}$  under the assumption that 99% of the degrees fall within the interval  $\langle k \rangle \pm 2.58\sqrt{\langle k \rangle}$ .

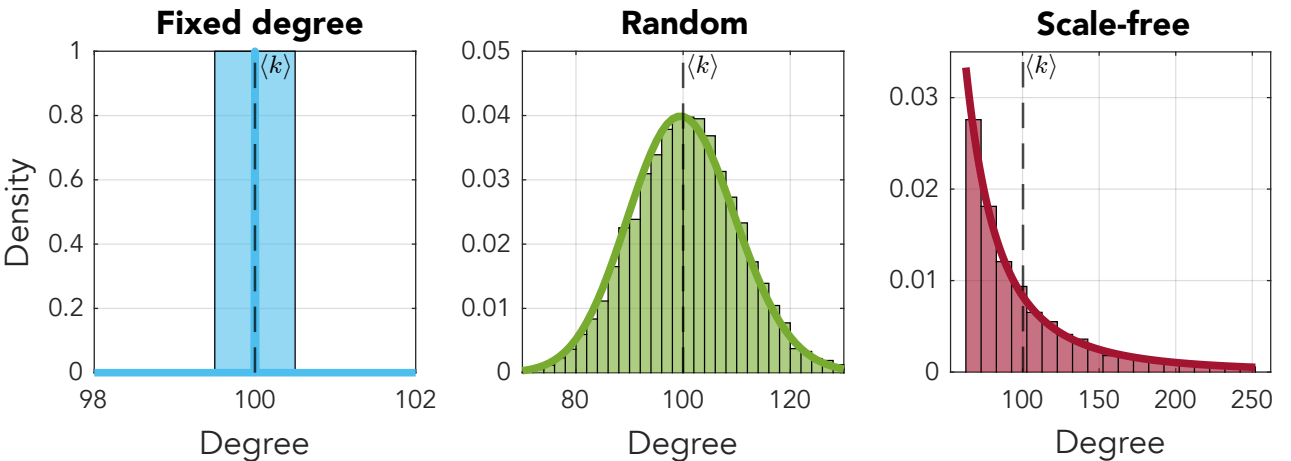


Figure 5: Univariate fixed-degree, random and scale-free distributions with the same average node degree  $\langle k \rangle = 100$ . The normalised histogram of  $k \in \mathbb{K}$  follows  $P(k)$  nicely as expected. Over the course of this work the colours used to indicate the different topologies will remain constant.

#### 4.4 Scale-free networks

What we can often observe in nature is the preferential attachment to nodes with a high degree [5]: the rich or famous tend to get more rich or famous. This trait is also described as the 80/20 rule by Pareto. Networks with this property consist of a small number of highly connected nodes, and a large number of low degree nodes. We can represent this with a power law distribution:

$$P(k) = Ak^{-\gamma} \quad \mathbb{K} = [k_{\min}, k_{\max}] \quad (16)$$

with  $A$  is a constant so that  $\sum_{k=1}^{\infty} P(k) = 1$ . We can also see that  $A \sum_{k=1}^{\infty} k^{-\gamma} = 1$  so that  $A = \sum_{k=1}^{\infty} k^{-\gamma} = 1/\zeta(\gamma)$ , the Riemann Zéta function [20].

Networks with a distribution like (16) are called *scale-free* networks, as they lack an internal scale to represent the magnitude of the network: we can observe (16) on different scales like the probability of two Hollywood actors appearing in a movie, or the connections between web pages on the internet [21]. One description that comes close is the *natural cutoff*  $k_{\max}$ , the expected degree of the largest degree in the network. As we only expect the largest hub to be the only hub in the domain  $[k_{\max}, +\infty]$ :

$$\int_{k_{\max}}^{\infty} P(k) dk = \frac{1}{N}$$

For (16) this results in:

$$k_{\max} = k_{\min} \cdot N^{\frac{1}{\gamma-1}} \quad (17)$$

which shows that there might be very large differences in size between the nodes. In practice, it is better to choose  $k_{\min}$  and  $k_{\max}$  and set  $P$  to zero outside of  $\mathbb{K}$ .

There are constraints on  $\gamma$  to yield a scale-free network. When  $0 < \gamma < 2$  the largest hub grows faster than  $N$ , so once its degree exceeds  $N - 1$  there are no more new nodes to connect to and the network will not be able to grow according to (16). A rigorous proof is given in [22]. For  $\gamma = 2$ , the system grows linearly, as we can see in (17). When  $2 < \gamma \leq 3$  we find the most scale-free networks, as for  $\gamma > 3$  hubs are not sufficiently large and numerous to have much influence on the network [20].

#### 4.5 Networks of theta neurons

The human brain can be seen as a graph, with neurons as graph nodes, where the pre- to post-synaptic relation models a directional edge in the network. These edges are usually unidirectional though it can happen that the post- reconnects to the presynaptic neuron. Using this knowledge, we can easily extend the model to networks of neurons:

$$\dot{\theta}_i = (1 - \cos \theta_i) + (1 + \cos \theta_i) \cdot [\eta_i + I_i(t)] \quad \theta_i \in \mathbb{T}^N \quad (18)$$

$$I_i(t) = \frac{\kappa}{\langle k \rangle} \sum_{j=1}^N A_{ij} \cdot \mathcal{P}_n(\theta_j) \quad (19)$$

where the excitability  $\eta_i$  allows neuron  $i$  to adjust in which regime it is situated, and  $\eta_i \sim g(\eta|\eta_0, \sigma)$ .  $\kappa$  is the *synaptic* or *coupling* strength, and  $\mathcal{P}_n(\theta) = a_n(1 - \cos \theta)^n$  models synaptic coupling by a pulse-shaped signal, emitted when a neuron fires. As discussed in Chapter 2, there are conversions from the action potential to a neurotransmitter and back, but this process will be captured by using only  $\mathcal{P}$  as the action potential and  $\kappa$  as the "efficiency" of the conversions.  $n$  models the sharpness of the pulse, and  $a_n$  is a normalisation constant so that  $\int_{\mathbb{T}} \mathcal{P}_n d\theta = 2\pi$ . We will take  $n = 2$  from here, as in [7, 15, 23].

In (18) we see everything come together: changes to the phase  $\theta_i$  are induced by  $\dot{\theta}_i$  which in turn depends on the bifurcation of  $\theta$  with magnitude  $I_i$  which depends on all neurons in the network.

Studying a set of differential equations like (19) is not feasible, as we are quickly approaching thousands of neurons. And in the end, the dynamics of a single neuron are not of interest. Instead, we wish to capture and study how the network behaves as a whole. One aspect, synchrony, can be captured by the Kuramoto order parameter:

$$Z(t) = \frac{1}{N} \sum_{j=1}^N e^{i\theta_j} \quad Z(t) \in \mathbb{C}_o \quad (20)$$

$Z$  is a complex variable, consisting of a radius  $r = |Z|$  and argument  $\psi = \arg(Z)$ , so that  $Z(t) = r(t)e^{i\psi(t)}$ . When all phases are uniformly distributed across the unit circle  $\mathbb{T}$ , then  $|Z| = 0$ , resulting in a network with no synchronisation. When all phases are exactly the same,  $|Z| = 1$ , the network is fully synchronised. (20) describes the *mean-field* of the network, a simpler model that describes the average behaviour of the whole network. Analysis is simply conducted either on  $|Z(t)|$  versus time, or in the complex unit circle as  $\text{Re}(Z(t))$  versus  $\text{Im}(Z(t))$ .

Different works on the dynamics of (20) have been published [15, 23], and we will build on that analysis in the following chapters.

## 5 Mean Field Reductions

### 5.1 The Ott-Antonsen manifold

The *mean-field reduction* (*MFR*) is a theory that predicts the dynamics of the order parameter (20). In [6, 24, 25] such a method was published for fully connected networks of indistinguishable oscillators with harmonic coupling. In [26] the authors extended their work to include networks with arbitrary degree distributions, applied to the Kuramoto model. Later this analysis was extended to networks of the Theta Neuron model [7]. We will now consider the limit  $N \gg 1$  and formulate an exact *MFR* for different types of networks, following the method in [7].

To simplify notation, the authors incorporate the network size in to  $P$  so that  $\sum_{\mathbf{k} \in \mathbb{K}} P(\mathbf{k}) = N$ . To specify the probability of a link from a node of degree  $\mathbf{k}'$  to one of degree  $\mathbf{k}$  we can define an assortativity function:

$$a(\mathbf{k}_j \rightarrow \mathbf{k}_i) = 0 \leq \frac{k_j^{\text{out}'} k_i^{\text{in}}}{N \langle k \rangle} \leq 1 \quad (21)$$

where we have chosen a neutral assortativity [7]. (21) is constrained so that the number of links in the network,  $N \langle k \rangle$ , remains constant [26]:

$$\sum_{\mathbf{k}' \in \mathbb{K}} \sum_{\mathbf{k} \in \mathbb{K}} P(\mathbf{k}') a(\mathbf{k}' \rightarrow \mathbf{k}) P(\mathbf{k}) = N \langle k \rangle$$

We can now assume that the state of all neurons can be represented by a probability density function  $f(\theta, \eta | \mathbf{k}, t)$ . Hence, the marginal distribution

$$\int_{\mathbb{R}} \int_{\mathbb{T}} f(\vartheta, \eta' | \mathbf{k}, t) d\vartheta d\eta'$$

gives the fraction of nodes of degree  $\mathbf{k}$  with a phase in  $\mathbb{T}$  at time  $t$ . Also, we assume  $\eta_i$  do not change over time, so that  $\int_{\mathbb{T}} f(\vartheta, \eta' | \mathbf{k}, t) d\vartheta = g(\eta | \mathbf{k})$  gives the excitability distribution.

To describe the global synchronisation of the network of theta neurons (18) we have introduced the order parameter  $Z(t)$ (20). It is now hypothesized that  $Z(t)$  can be approximated by a mean-field order parameter, defined by the continuum limit:

$$\bar{Z}(t) = \frac{1}{N} \sum_{\mathbf{k} \in \mathbb{K}} P(\mathbf{k}) \int_{\mathbb{R}} \int_{\mathbb{T}} f(\vartheta, \eta' | \mathbf{k}, t) e^{i\vartheta} d\vartheta d\eta' \quad (22)$$

Here,  $f$  is constrained by a continuity equation, as the number of oscillators is conserved:

$$\frac{\partial f}{\partial t} + \frac{\partial}{\partial \theta} (v_\theta f) = 0 \quad (23)$$

with  $v_\theta$  a continuum version of (18):

$$v_\theta = (1 - \cos \theta) + (1 + \cos \theta)[\eta + I(\mathbf{k}, t)]$$

$$I(\mathbf{k}, t) = \frac{\kappa}{\langle k \rangle} \sum_{\mathbf{k}' \in \mathbb{K}} P(\mathbf{k}') a(\mathbf{k}' \rightarrow \mathbf{k}) \times \left[ \int_{\mathbb{R}} \int_{\mathbb{T}} f(\vartheta, \eta' | \mathbf{k}', t) a_n (1 - \cos \vartheta)^n d\vartheta d\eta' \right]$$

In [6] it is shown that there exists a manifold of invariant probability densities for the continuity equation. The exact *MFR* is obtained by expanding  $f$  as a Fourier series, and expanding the pulse  $\mathcal{P}_n$  using the binomial theorem. When assuming  $\eta_i$  is distributed according to a Lorenz distribution:

$$g(\eta | \mathbf{k}) = \frac{1}{\pi} \frac{\sigma(\mathbf{k})}{(\eta - \eta_0(\mathbf{k}))^2 + \sigma(\mathbf{k})^2} \quad (24)$$

the set of reduced equations then takes a particularly simple form, as (22) can be evaluated the poles of  $g$  using the Cauchy residue theorem for the integration of complex variables and find a closed form expression. We can now capture the dynamics by  $z(\mathbf{k}, t)$ , the mean-field variable for nodes of degree  $\mathbf{k}$ :

$$\begin{aligned} \frac{\partial z(\mathbf{k}, t)}{\partial t} &= -i \frac{(z(\mathbf{k}, t) - 1)^2}{2} + \frac{(z(\mathbf{k}, t) + 1)^2}{2} \cdot I(\mathbf{k}, t) \quad z(\mathbf{k}, t) \in \mathbb{C}_o^{M_k} \\ I(\mathbf{k}, t) &= -\sigma(\mathbf{k}) + i\eta_0(\mathbf{k}) + iH_2(\mathbf{k}, t) \\ H_2(\mathbf{k}, t) &= \frac{\kappa}{\langle k \rangle} \sum_{\mathbf{k}' \in \mathbb{K}} P(\mathbf{k}') a(\mathbf{k}' \rightarrow \mathbf{k}) \cdot \left( 1 + \frac{z(\mathbf{k}', t)^2 + (z(\mathbf{k}', t)^c)^2}{6} - \frac{4}{3} \operatorname{Re}(z(\mathbf{k}', t)) \right) \end{aligned} \quad (25)$$

with  $z^c$  the complex conjugate.  $H$  is a legacy term and has been computed in [23]. The mean-field order parameter can now be expressed in terms of  $z(\mathbf{k}, t)$ . Using the constraints on  $f$  and  $g$  we can now solve (22) as:

$$\bar{Z}(t) = \frac{1}{N} \sum_{\mathbf{k}} P(\mathbf{k}) z(\mathbf{k}, t) \quad \bar{Z}(t) \in \mathbb{C}_o \quad (26)$$

which clearly reflects the network architecture through  $P(\mathbf{k})$ , as in the limit, this is the number of neurons of degree  $\mathbf{k}$  that are present in the network. The mean-field dynamics of the whole network are therefore equal to a weighed average of the degree dynamics of the nodes with a unique degree. We have now formulated the evolution on the invariant manifold by a reduced set of ordinary differential equations. The *MFR* is computationally efficient, and in [7] many methods for improving this efficiency further are treated.

## 5.2 Simplifications for fixed-degree networks

In the case of a fixed-degree network, every node has  $\deg(\theta_i) = (\langle k \rangle, \langle k \rangle)$  so:

$$\frac{1}{\langle k \rangle} \sum_{\mathbf{k}' \in \mathbb{K}} P(\mathbf{k}') a(\mathbf{k}' \rightarrow \mathbf{k}) = \frac{1}{\langle k \rangle} N \left( \frac{\langle k \rangle \langle k \rangle}{N \langle k \rangle} \right) = 1$$

This is an identical formulation as in [15] and [23] and for any fixed-degree network, eqs. (25) and (26) reduce to a single complex differential equation:

$$\dot{Z}(t) = -i \frac{(Z - 1)^2}{2} + \frac{(Z + 1)^2}{2} \cdot \left( -\sigma + i\eta_0 + i\kappa \cdot \left( 1 + \frac{Z^2 + (Z^c)^2}{6} - \frac{4}{3} \operatorname{Re}(Z) \right) \right) \quad (27)$$

This is an identical formulation for any fixed-degree network, and as it is a complex-valued function, the reduced system is two-dimensional with three bifurcation parameters  $\eta_0, \sigma$  and  $\kappa$ , [15, 23]. We will start our analysis with (27).

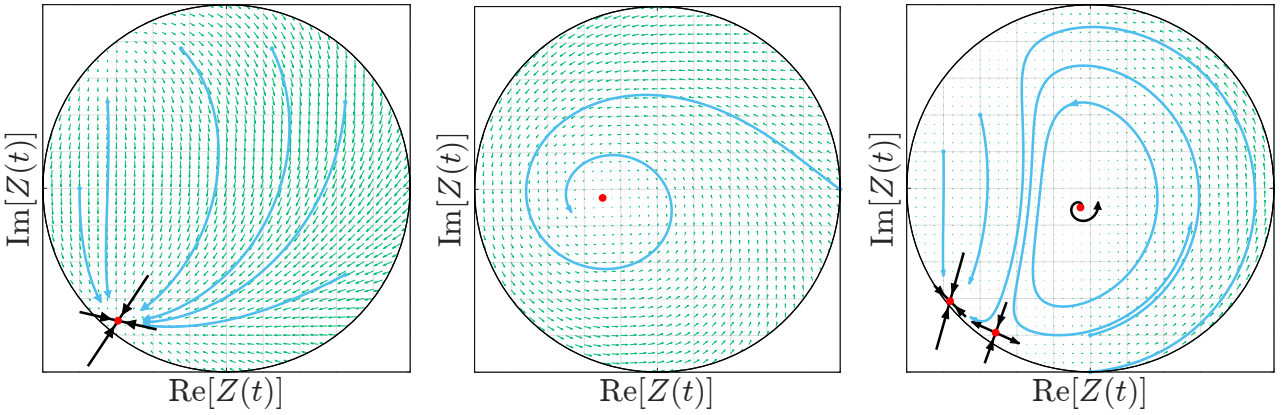
Three distinct macroscopic states can be identified. In the partially synchronous rest state (*PSR*) we can observe in Figure 6a,  $Z(t)$  settles onto a stable node. Most neurons can be found in a resting state  $\eta_0 + \sigma \lesssim 0$ , and inhibit one another through  $\kappa < 0$ . Most neurons are therefore inactive, though some spiking neurons from the tail of  $g$  are present but have a negligible effect.

In Figure 6b we can observe a partially synchronous spiking (*PSS*) state, where we can see how  $Z(t)$  settles onto a stable focus. This happens predominantly when  $\eta_0 - \sigma \gtrsim 0$  and most neurons inherently spike, with the coupling being either excitatory or weakly inhibitory. Although most neurons are active, the network is partially synchronous and organized such that phase cancellation

occurs by continuous spiking among the neurons.

Lastly, in the collective periodic wave state (*CPW*) we can observe a limit cycle of the mean field, in Figure 6c. Most neurons are active and inhibitory:  $\eta_0 > 0$  and  $k < 0$ . The collective oscillation emerges from the interplay between the neurons' inherent tendency to spike and the strong suppressive network interaction. *CPW* states are mediated through Hopf bifurcations and homoclinic bifurcations of  $Z(t)$ . We can also see the occurrence of a saddle-node bifurcation in the lower hand corner, for low  $\sigma$ . We will continue to study the *CPW* due to their interesting properties.

A more detailed discussion of the different regimes and bifurcations can be found in [15].



(a) PSR state for  $\eta_0 = -0.9, \sigma = 0.8$  and  $\kappa = -2$ . The mean field settles onto a stable node.

(b) PSS state for  $\eta_0 = 0.5, \sigma = 0.7$  and  $\kappa = 2$ . The mean field settles onto a stable focus.

(c) CPW state for  $\eta_0 = 10.75, \sigma = 0.5$  and  $\kappa = -9$ . The mean field settles onto a stable limit cycle.

Figure 6: Three macroscopic states observed in the *MFR* inside the imaginary unit circle  $|Z(t)| = 1$ . Green arrows mark the phase space vector field and blue trails mark solution curves. Red points indicate equilibrium points, with black arrows marking the direction of the eigenvectors in that point, scaled according to the magnitude of the corresponding eigenvalues. This information is found from the Jacobian, which we will discuss in Chapter 6.

### 5.3 Implications and challenges of the *MFR*

The advantages of using the *MFR* can be found in the number of equations we now have left to investigate. As there are  $M_k$  equations in (25), instead of  $N$  equations for  $N$  neurons, the reduction becomes more and more efficient for larger networks. As we have seen in (27) this yields a single equation for a fixed-degree network, as all neurons have the same degree.

While the *MFR* gives us the opportunity to use any arbitrary univariate distribution  $P(k)$  for undirected, symmetric networks or any bivariate distribution  $P(\mathbf{k})$  for directed, asymmetric networks, none of the publications on the *MFR* have treated directed networks. The challenge is that the support  $\mathbb{K}$  is a much larger set, as  $\mathbb{K} = \mathbf{k}^{\text{out}} \times \mathbf{k}^{\text{in}}$ . For example, the scale-free distribution (16) has  $M_k = k_{\max} - k_{\min}$  number of degrees in its support. An example would be  $M_k = 1250$ , [7]. For 10.000 neurons, that is a reduction of 87,5%. When we wish to extend (16) to a bivariate distribution,  $M_k$  grows to  $(k_{\max} - k_{\min})^2$ . A bivariate distribution would therefore need about  $1.56 \times 10^6$  equations for 10.000 neurons. It is not feasible to solve this many equations at once.

## 6 Investigation: Mean Field Reductions for undirected graphs

We will now investigate the questions that were raised after deriving the *MFR*. How do we deal with the curse of dimensionality concerning the degree distribution? There are also other questions to be answered. If the synchronisation dynamics of the network of Theta neurons (18) can be predicted by the Ott-Antonsen reductions eqs. (25) to (27), then it can also be measured by the order parameter (20). These systems describe the same quantity, but how can we show that?

### 6.1 Directed graphs as permutations

So how can we use the *MFR* efficiently when the network is a directed graph with an asymmetrical adjacency matrix? Let's investigate.

- Sampling  $k^{\text{in}}$  and  $k^{\text{out}}$  from a bivariate distribution requires us to find the marginal distribution of  $P$  for  $k^{\text{in}}$ , sampling  $k_i^{\text{in}}$ , and then sampling  $k_j^{\text{out}}$  from  $P$  while keeping  $k_i^{\text{in}}$  fixed. This is a cumbersome process. And what relation would there be between  $k^{\text{in}}$  and  $k^{\text{out}}$ ?
- However, if we assume that the marginal distributions for  $k^{\text{in}}$  and  $k^{\text{out}}$  are independent, there is a simplification to be found. We can even assume that the two marginal distributions are identical univariate distributions.
- Hence, we can sample  $k^{\text{in}}$  from a univariate distribution and find  $k^{\text{out}} = F(k^{\text{in}})$  so that the total number of links remains constant. This is an important trait, as we do not have to rely on the sheer size of the network to yield a constant number of links on average.

This hypothesis can be tested: we assume that  $P(\mathbf{k}) = P(k^{\text{in}}) \cdot P(k^{\text{out}})$  so that  $P$  consists of two identical and independent distributions, given by the distributions presented in Chapter 4. Then, we sample  $k^{\text{in}} \sim P(k^{\text{in}})$  and perform a permutation to find the in- and out-degrees  $k_j$  for each node  $j$ . The surface given by  $P(\mathbf{k})$  and the histogram of  $k_j$  have been plotted in Figure 7. As we can see, the variates follow the distribution well.

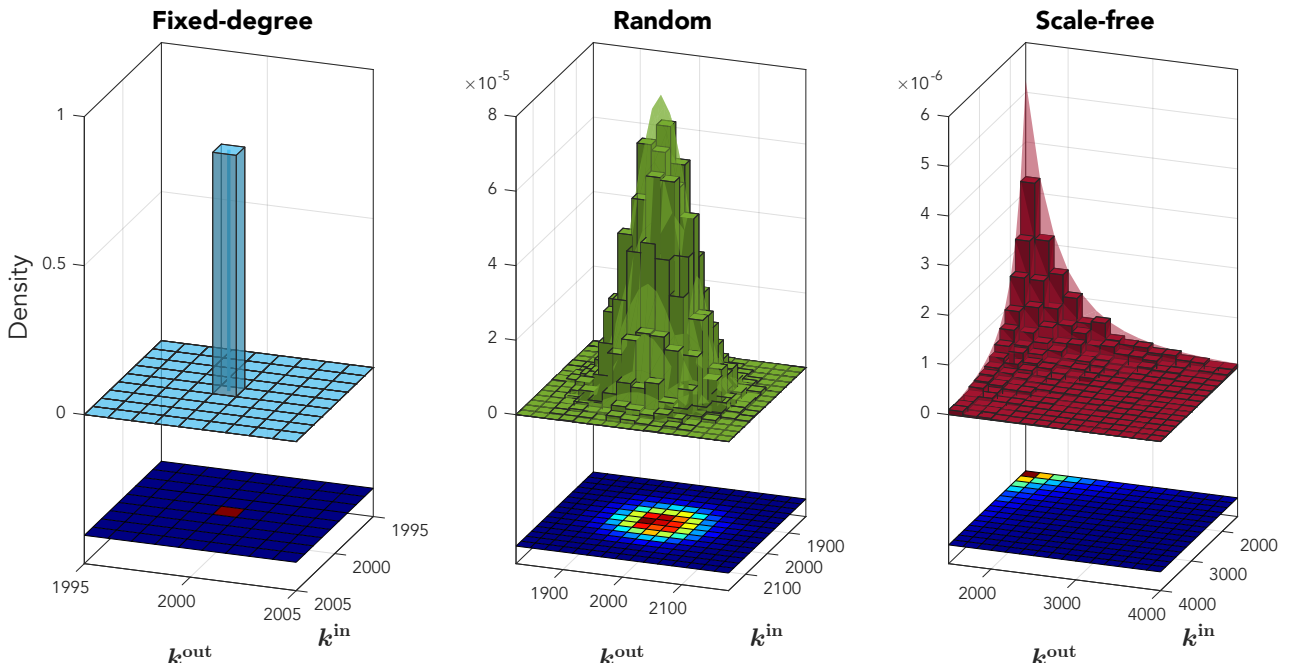


Figure 7: Bivariate distributions for different network topologies, using  $10^4$  number of samples. The surface given by  $P(\mathbf{k})$  is well approximated by the histogram of variates sampled from a univariate distribution, used as the marginal distribution.  $\langle k \rangle = 2 \times 10^3$  for all topologies,  $p \approx 0.2$  for the random network and  $\gamma = 4.3$  for the scale-free network.

However, the problem remains the same:  $\mathbb{K}$  is too large to simulate the dynamics of the network. What we can do, is use  $P(k)$  in the Ott-Antonsen reduction for a symmetric network, and observe how much the dynamics of the asymmetric network differ.

## 6.2 Building the adjacency matrix

If we want to simulate the network of theta neurons (19) we need to construct the adjacency matrix. We can find an exact solution for  $A$  given the degree vectors in (12).  $A_{ij}$  represents a directed graph, but  $A_{ij} \neq A_{ji}$  is not a necessary condition. For the elements of  $A_{ij}$  we need to find  $N^2$  number of variables. We have the following constraints:

1. The column- and row-sums of  $A_{ij}$  must be equal to  $k^{\text{in}}$  and  $k^{\text{out}}$ , see (10).  $2N$  constraints.
2. Self-coupling is mandatory:  $A_{ii} = 1$ .  $N$  constraints. [7]
3. The total number of links is constant:  $\sum_{i=1}^N k_i^{\text{in}} \equiv \sum_{j=1}^N k_j^{\text{out}} \equiv \sum_{i,j=1}^N A_{ij}$ . 1 constraint.

This means that there are  $N^2 - (3N + 1)$  variables to find. Once a solution has been found,  $A_{ij}$  can be switched with element  $A_{ic}$  if  $A_{ij} \neq A_{ic}$  and  $A_{rj}$  with  $A_{rc}$ , which yields another feasible solution. The solutions to this problem are thus bound by permutation symmetry. The number of switches one can make is high, and therefore we can simply try a stochastic approach to obtain  $A$ :

1. Choose a random row  $i \in [1, N]$ .  $A_{i,i} = 1$ , so we need  $m = k_i^{\text{in}} - 1$  elements that are 1.
2. Perform  $F(k_j^{\text{out}}, j \neq i)$  and therein find the indices  $\ell$  of the  $m$  first largest elements.
3. Set  $A_{il} = 1 \forall l \in F^{-1}(\ell)$ .

Algorithms that find the largest value in a vector start from the first or the last element. The permutation in step 2 allows us to find different maxima every time by shuffling the row, which greatly reduces the event that constraint 1 does not hold. In practice, this stochastic method finds a solution for  $A$  within 5 tries.

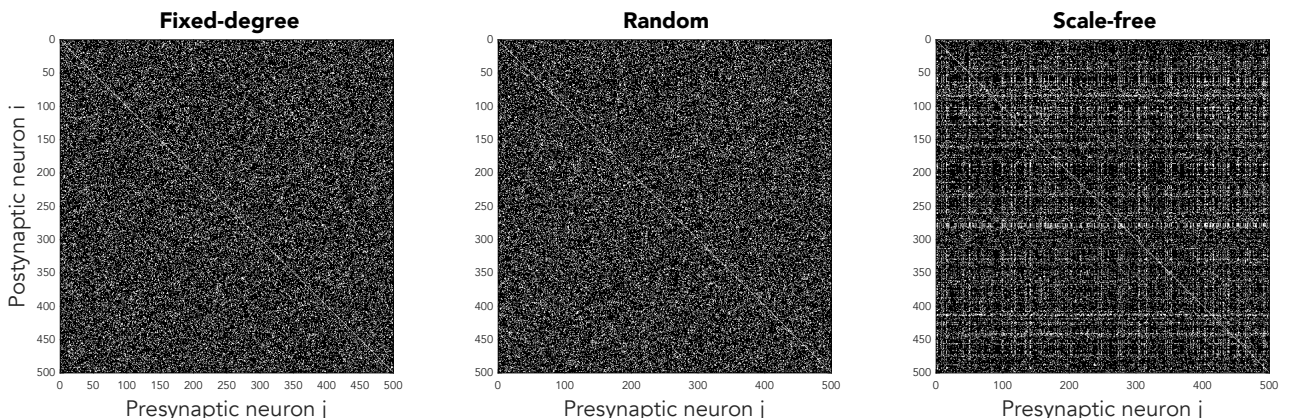


Figure 8: Adjacency matrices for different types of networks with  $N = 500$  and  $\langle k \rangle = 100$ . We can see how the fixed-degree network is quite homogeneous, while the random network shows some more clustering. The scale-free network has a low number of nodes with a very high degree, which is why we see vertical and horizontal stripes in the adjacency matrix.

## 6.3 Initial conditions: analytical versus numerical approaches

As our goal is to compare theory and simulations, we need to be able to start both at the exact same condition. This notion requires us to transform between the three number sets that our dynamics are described in:  $\theta \in \mathbb{T}^N$ ,  $z \in \mathbb{C}_o^{M_k}$  and  $Z, \bar{Z} \in \mathbb{C}_o$ . It is really only necessary to find a

transformation that holds accurately for  $t = 0$ , as the distribution of  $\theta$  and  $z$  over their number set is unknown, but we assume they converge to that distribution when the systems are computed. As we can optimally study the behaviour of  $Z$  and  $\bar{Z}$  in the complex unit circle, the most important transformations are those that yield  $\theta$  and  $z$  from  $Z$  and  $\bar{Z}$  respectively. Hence, we can start our simulations anywhere in  $\mathbb{C}_o$ , close to the limit cycle in Figure 6c for example. Our analysis will benefit a great deal from this advantage.

Let us start with the simplest transformation. Given an initial phase angle  $\theta_i(0)$  or initial degree dynamics  $z(\mathbf{k}, 0)$  we wish to find their resulting description in the complex unit circle. Mapping operations onto the order parameter is straightforward using (20) and (26):

$$\theta_i(0) \longrightarrow Z(0) = \frac{1}{N} \sum_{j=1}^N e^{i\theta_j(0)} \quad (28)$$

$$z(\mathbf{k}, 0) \longrightarrow \bar{Z}(0) = \frac{1}{N} \sum_{\mathbf{k} \in \mathbb{K}} P(\mathbf{k}) z(\mathbf{k}, 0) \quad (29)$$

Here we can immediately see that information about the distribution of  $\theta$  and  $z$  is lost when taking the (weighed) average.

Starting from an initial synchronization  $Z(0)$  and taking the inverse transformation, we can make use of the fact that a set of identical values has an average equal to that value. This is simple for  $\theta_i(0)$ : we can take all phase angles to be the same at  $t = 0$ . For  $z(\mathbf{k}, 0)$  we have a weighed average which we need to invert, while making sure that the whole sums up to  $N$  by multiplying with the total number of neurons  $n(\mathbf{k})$  of degree  $\mathbf{k}$ :

$$Z(0) \longrightarrow \theta_i(0) = -i \cdot \log(Z(0)) \quad (30)$$

$$Z(0) \longrightarrow z(\mathbf{k}, 0) = \frac{Z(0) \cdot n(\mathbf{k})}{P(\mathbf{k})} \quad (31)$$

It is necessary to include  $n(\mathbf{k})$ , as  $P$  is only accurate in the limit that  $N \gg 1$ . This approach only alters the magnitude of  $Z(0)$ , so that  $z(\mathbf{k}, 0)$  will be distributed on a line through  $Z(0)$ . Then, transforming between  $\theta_i$  and  $z(\mathbf{k})$ , we need to filter  $\theta_i$  per degree as there exist  $n(\mathbf{k})$  number of nodes with  $\deg(\theta_i) = \mathbf{k}$ :

$$z(\mathbf{k}, 0) \longrightarrow \theta_i(0) = -i \cdot \log\left(\frac{z(\mathbf{k}) \cdot P(\mathbf{k})}{n(\mathbf{k})}\right) \quad \forall \theta \in \{\theta \mid \deg(\theta) = \mathbf{k}\} \quad (32)$$

$$\theta_i(0) \longrightarrow z(\mathbf{k}, 0) = \sum_{\mathbf{k}} e^{i\vartheta_{\mathbf{k}}} \quad \forall \vartheta_{\mathbf{k}} \in \{\vartheta_{\mathbf{k}} = \sum_{\mathbf{k}} \theta \mid \deg(\theta) = \mathbf{k}\} \quad (33)$$

The relations derived here raise problems when  $P(\mathbf{k})$  spans different orders of magnitude. (31) does not bound  $z$  to its set, so it might occur that the distribution of  $z$  has values outside of the complex unit circle. However, transforming back to  $\bar{Z}$  will always be correct. This problem does not occur for  $\theta$ , as  $\mathbb{T}$  is a one-parameter group because multiplication and division of elements in the group remain in the group. Let us look at the example in Figure 9, where we are trying to find  $z(\mathbf{k}, 0)$  so that  $\bar{Z}(0)$  is equal to the desired initial condition  $Z(0) = -0.2 + i0.8$ , using a scale-free topology.

When simply taking all  $z(\mathbf{k}, 0) = Z(0)$ , there is a slight offset between  $Z(0)$  and  $\bar{Z}(0)$ . However, the dynamics are well-behaved and the end-state is almost a smooth curve. One can really interpret this curve as the attractive manifold of the Ott-Antonsen reduction. This method is an easy way

of quickly coming up with an initial condition, without requiring any computation. In general, this yields quite a good approximation.

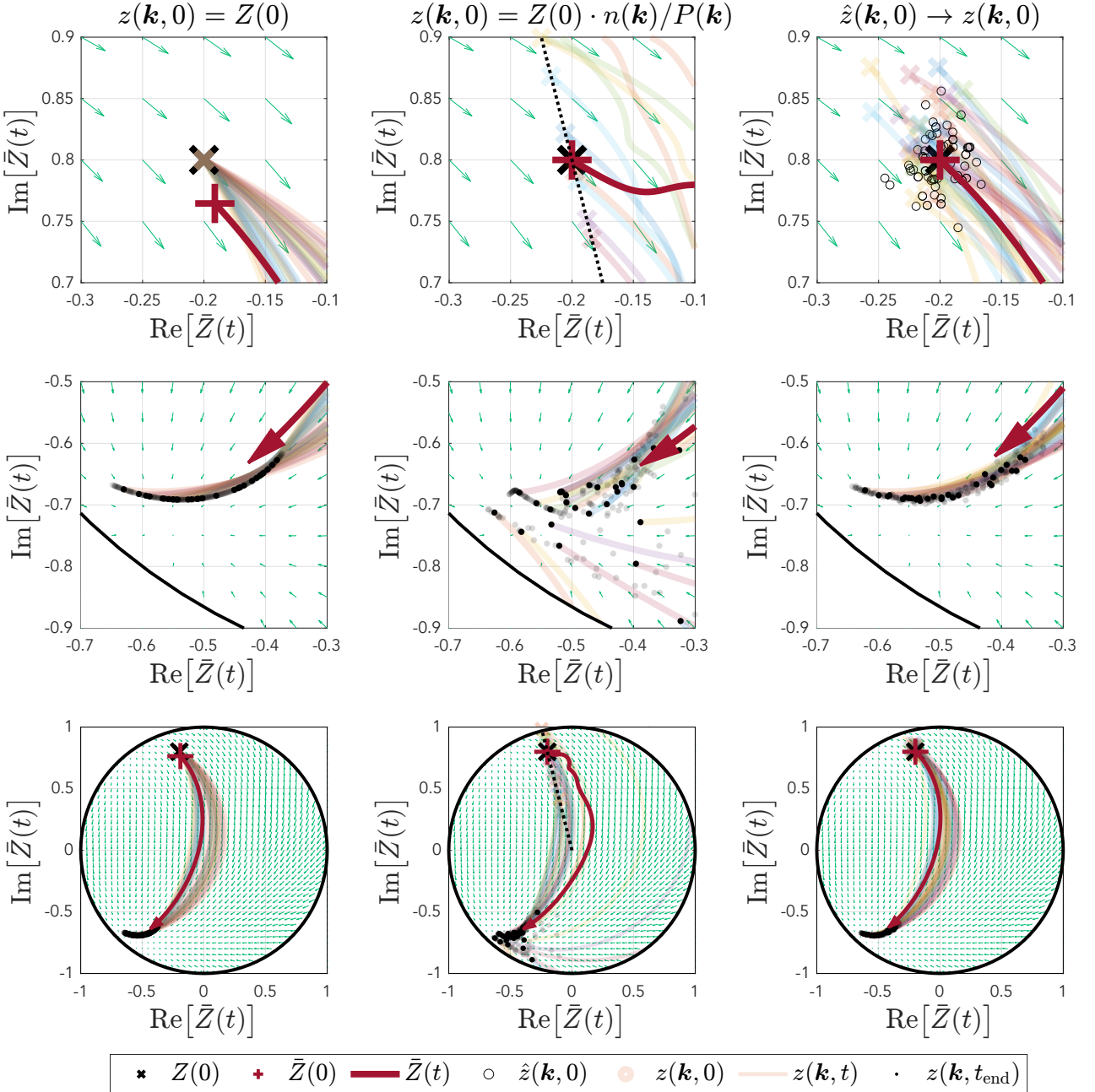


Figure 9: Simulation of 1000 neurons in a scale-free network. Example on the importance of accurate initial conditions. A scalefree network is used to show the outcome of different strategies of initialising the network. Left: the initial condition is not correct, but it yields very smooth dynamics. Middle: the initial condition is correct, but it does not yield smooth dynamics. Right: the initial condition is correct, and it yields smooth dynamics.

When using (29), we can see that the initial conditions lie on a straight line through the origin indeed, and that  $\bar{Z}(0)$  is exactly equal to  $Z(0)$ . When a given  $\mathbf{k}$  yields a small  $P(\mathbf{k})$ ,  $z(\mathbf{k}, 0)$  will be scaled away from the origin. This means that the dynamics of nodes of that degree are not well represented. However, their contribution to  $\bar{Z}$  in (26) is small, so sometimes these effects cancel out and the dynamics are in fact quite smooth. However, we can see that in our example the

dynamics are not represented well, resulting in large errors after conception and a more random end-state. We do expect these effects to cancel out after longer periods and for larger  $N$ , as the manifold is attractive and larger networks cancel out outliers, but our aim is to be as precise as possible from  $t = 0$ .

When trying to address the problems that are encountered here, we can try and find the distribution of  $z(\mathbf{k}, 0)$  numerically by solving for the root of  $f(z) = \|Z(0) - \bar{Z}(0)\|$  (where  $\bar{Z}$  is computed from  $z$ ) under the constraint that  $|z| \leq 1$ , starting from an initial guess  $\hat{z}$ , clustered around  $Z(0)$ . The resulting initial distribution is also quite clustered but as it is mostly a result of the constraint, we are more interested in the end-state, which shows a lot of improvements over the second method. The initial conditions are exact (up to  $10^{-6}$ ) and the dynamics are smooth, which makes this method the most desirable. However, convergence can be very slow for scale-free networks, and the complexity of the system to solve scales with  $\sim N^2$ . It is therefore necessary to judge which of the three methods to use when performing a new simulation.

#### 6.4 Final conditions

Given that the final condition of the system is such a particular smooth curve, we can try and understand what kind of distribution  $z$  follows on that curve. In Figure 10 we have made a different networks converge to a stable node in the *PSR* state until changes to the system were smaller than a tolerance. We can see that the final condition of  $z$  is close to the final condition of  $\bar{Z}$ . If we divide the length of the curve into equal parts, we can count how many  $z$  can be found in each interval. The resulting distributions difficult to interpret, but we can see some traits of their respective degree distributions, though the likeness is not very high.

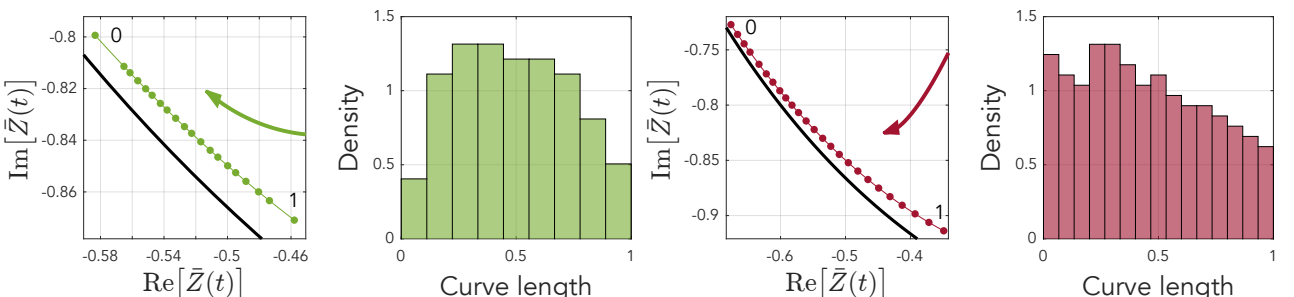


Figure 10: Final conditions of  $z$  for the *PSR* state, represented by 20 equally spaced indices and the resulting histogram. Both the random and scale-free network topologies show that the final conditions of  $z$  are a smooth curve, and that points on that curve have a particular distribution over the length of the curve.

For other macroscopic states the distributions of  $z$  across its final condition are quite similar as presented here. However, when the scale-free network has converged to the stable focus in the *PSS* state, the final condition is a highly convoluted spiral, which is difficult to interpret. What is important though, is that there is a definite structure to be found in the final condition as well.

#### 6.5 Commutativity of complex vectors

It is important to notice that in (25) and (26) and many other equations in this work, we compute an inner vector product, which is non-commutative for complex numbers:

$$a \cdot b = \overline{b \cdot a} \quad a, b \in \mathbb{C}_o^r \quad (34)$$

This is the result of the *Conjugate* or *Hermitian* symmetry of the inner product. This is especially important in the MATLAB implementation, as one needs to remain consistent with left-hand or right-hand products.

## 6.6 Fixpoint iteration

In [7] a fixpoint iteration is suggested to find attractive fixpoints of the system (25). If we set  $\frac{\partial z(\mathbf{k}, t)}{\partial t} = 0$  we can solve the following system:

$$\begin{aligned} i \frac{(z(\mathbf{k}, t) - 1)^2}{2} &= \frac{(z(\mathbf{k}, t) + 1)^2}{2} \cdot I(\mathbf{k}) \\ i \left( \frac{z(\mathbf{k}, t) - 1}{z(\mathbf{k}, t) + 1} \right)^2 &= I(\mathbf{k}) \\ \frac{z(\mathbf{k}, t) - 1}{z(\mathbf{k}, t) + 1} &\equiv b(\mathbf{k}, t) \\ z(\mathbf{k}, t) - 1 &= b(\mathbf{k}, t)z(\mathbf{k}, t) + b(\mathbf{k}, t) \\ z(\mathbf{k}, t) \cdot (1 - b(\mathbf{k}, t)) &= b(\mathbf{k}, t) + 1 \end{aligned}$$

We can then obtain the stable equilibria from:

$$ib(\mathbf{k}, t)^2 = I(\mathbf{k}) \quad z(\mathbf{k}, t)_\pm = \frac{1 \pm b(\mathbf{k}, t)}{1 \mp b(\mathbf{k}, t)} \quad (35)$$

where the signs are chosen so that  $|z(\mathbf{k}, t)| \leq 1$ . This works well, and in general this method converges fast.

## 6.7 A Newton-Raphson iteration for all fixpoints

The fixpoint iteration (35) only gives us the stable equilibria of the MFR. We can obtain all equilibria and their stability through the Jacobian from a Newton-Raphson iteration, which has been described in A.4. The Jacobian would be a  $M_{\mathbf{k}} \times M_{\mathbf{k}}$  matrix, as we have  $M_{\mathbf{k}}$  unique degrees in the network, and we need to take the derivate of one with respect to each other. However, finding the Jacobian is a challenge, as (25) is non-holomorphic:  $H_2(\mathbf{k}, t)$  does not satisfy the Cauchy-Riemann equations. We can show this by separating  $z$  into its real and imaginary part and expressing  $H_2(\mathbf{k}, t)$  as two real-valued functions  $u$  and  $v$ :

$$\begin{aligned} z(\mathbf{k}, t) &= x(\mathbf{k}, t) + i \cdot y(\mathbf{k}, t) \quad x, y \in \mathbb{R}^{M_{\mathbf{k}}} \\ f(z(\mathbf{k}, t)) &= u(x(\mathbf{k}, t), y(\mathbf{k}, t)) + iv(x(\mathbf{k}, t), y(\mathbf{k}, t)) \\ &= \frac{\kappa}{\langle k \rangle} \sum_{\mathbf{k}'} P(\mathbf{k}') a(\mathbf{k}' \rightarrow \mathbf{k}) \cdot \left( 1 + \frac{z(\mathbf{k}', t)^2 + (z(\mathbf{k}', t)^c)^2}{6} - \frac{4}{3} \operatorname{Re}(z(\mathbf{k}', t)) \right) \\ &= \frac{\kappa}{\langle k \rangle} \sum_{\mathbf{k}'} P(\mathbf{k}') a(\mathbf{k}' \rightarrow \mathbf{k}) \cdot \left( 1 + \frac{x(\mathbf{k}', t)^2}{3} - \frac{4}{3} x(\mathbf{k}', t) \right) \end{aligned}$$

This leaves us with only  $u$  defined as a real-valued function, so that the Cauchy-Riemann equations do not hold as  $v$  is zero. Thus we cannot express the Jacobian as a matrix of complex numbers.

Instead, we must think of  $z$  as a vector of real and imaginary parts and express it as  $z(\mathbf{k}, t) = [x(\mathbf{k}, t), y(\mathbf{k}, t)]$ . We can then interweave the two parts in the Jacobian, forming a  $2M_{\mathbf{k}} \times 2M_{\mathbf{k}}$  matrix of real values. For fixed-degree networks this is easy, and the approach yields the well-known 2 by 2 Jacobian, which has been used in Figure 6 to signify the stability of the equilibrium points and the magnitude and direction of the eigenvalues.

However, for the typologies with more than one unique degree in the network, this approach did not yield stable results. It is either the derivation or the execution that is flawed, though the mistake could not be found. For now, we will revert to the fixed point iteration (35) to find stable equilibria of the system.

## 6.8 Fixed-degree networks as a baseline

Now we have all the necessary tools to simulate networks of theta neurons: the adjacency matrix, and an understanding of the initial conditions. First, we will use a fixed-degree network, as this is the most simple instance of the different topologies. As all nodes have the same degree, the dynamics of a symmetric and asymmetric fixed-degree network ought to be identical. The results are shown in Figure 11. There are small differences between simulation and theory, but these are most likely due to a finite network size and a finite integration step. As a matter of fact, the mean-field systems (26) and (27) yield the exact same behaviour. This test benchmarks the lowest amount of error we can observe between simulation and theory, as for fixed-degree networks (25) consists of a single equation.

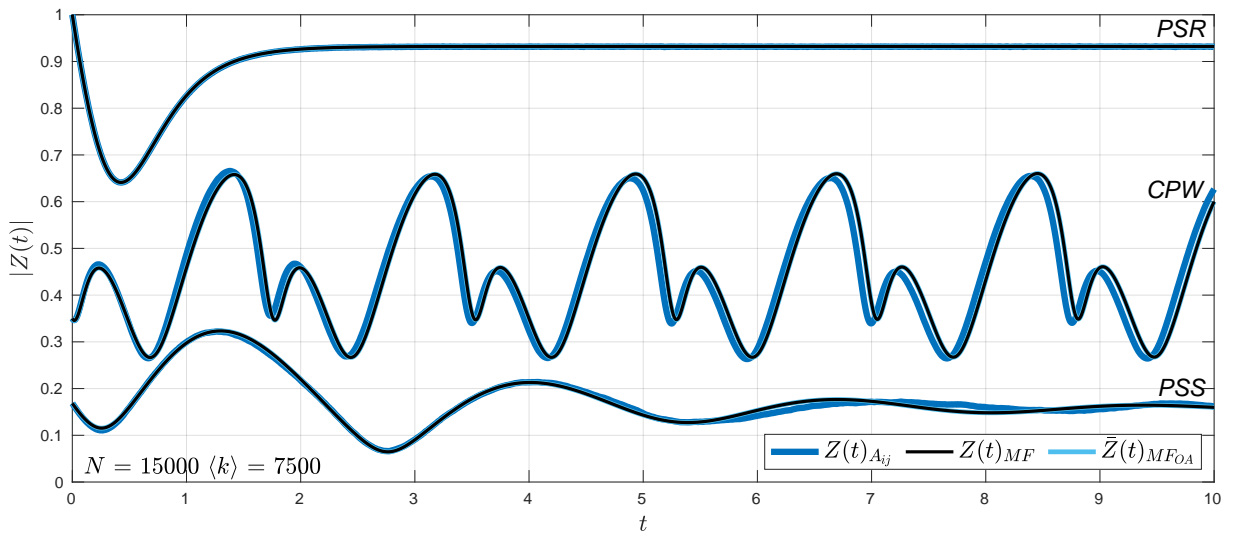
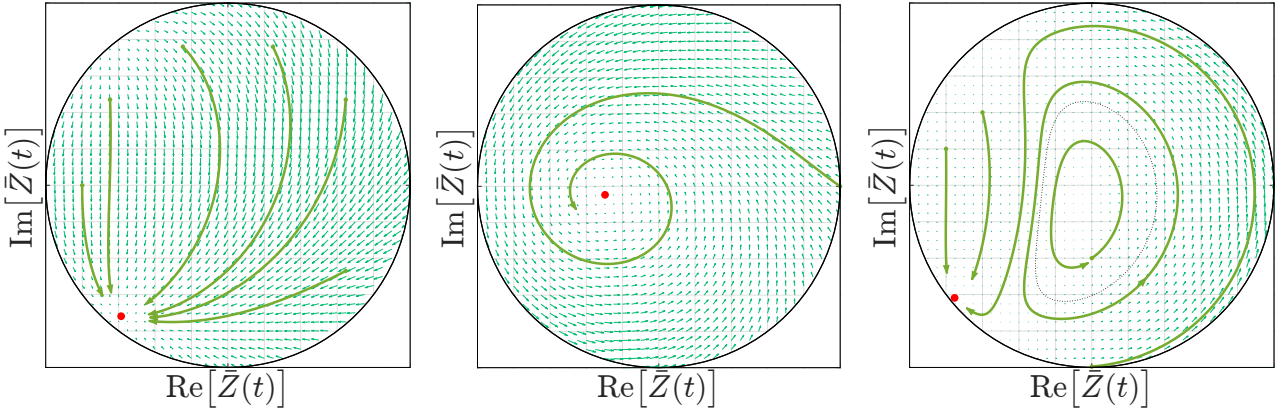


Figure 11: Comparison of the simulation of a fixed-degree network of Theta neurons and the Ott-Antonsen theory by the magnitude of the order parameter. We observe that the same three macroscopic states are found by the three descriptions.

## 6.9 Results for arbitrary network topologies

The dynamics of random networks seem to be very similar to fixed-degree networks, when looking at the unit circle. We can see in Figure 12c that the limit cycle is a little larger. When looking at the dynamics over time the results in Figure 13 are also consistent, with a little more deviation between simulation and theory in the CPW state.



(a) PSR state for  $\eta_0 = -0.9, \sigma = 0.8$  and  $\kappa = -2$ . The mean field settles onto a stable node.

(b) PSS state for  $\eta_0 = 0.5, \sigma = 0.7$  and  $\kappa = 2$ . The mean field settles onto a stable focus.

(c) CPW state for  $\eta_0 = 10.75, \sigma = 0.5$  and  $\kappa = -9$ . The mean field settles onto a stable limit cycle.

Figure 12: Three macroscopic states observed in the *MFR* inside the imaginary unit circle  $|Z(t)| = 1$ . Green arrows mark the phase space vector field and blue trails mark solution curves. Red points indicate equilibrium points, found by the fixed-point iteration. The dotted line in the *CPW* state is the limit cycle of the fixed-degree networks, added for reference.

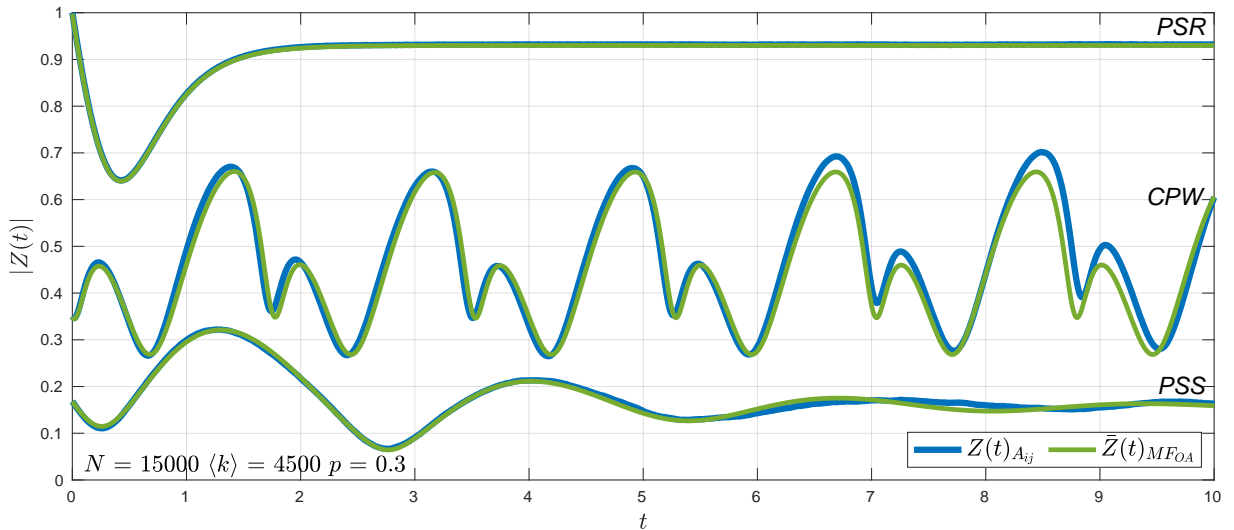
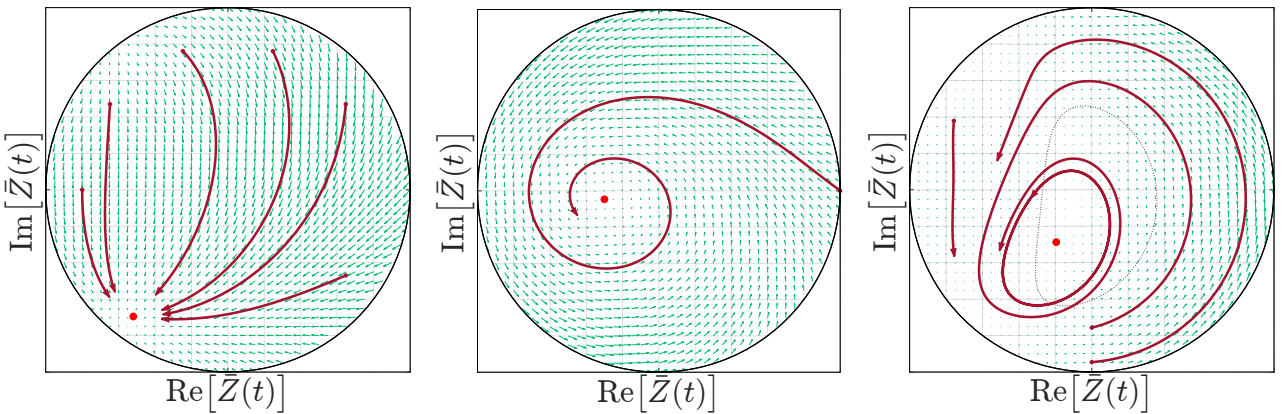


Figure 13: Comparison of the simulation of a random network of Theta neurons and the Ott-Antonsen theory by the magnitude of the order parameter.

For scale-free networks, we can see that again the three macroscopic states continue to exist, Figure 14. However, it seems like there is a fairly large discrepancy between symmetric and asymmetric networks, in Figure 15. The stable node in the *PSR* state is found at different locations, and the limit cycle in the *CPW* state seems to be very different, but with a similar period. Indeed, if we look at the limit cycle to which the dynamics are attracted to in Figure 16 we can indeed see two distinct cycles.

This means that due to its topology, the scale-free network cannot be represented by a symmetric variant. The degree distribution is asymmetric, and this likely causes the asymmetry observed here. Another observation is that now the fixed-point iteration finds the centre of the limit cycle as a stable equilibrium. The limit cycle has always been observed to be attractive, so a stable equilibrium

within would require another unstable limit cycle around the equilibrium. We will regard this as an error, as we do not have the Jacobian to verify the stability of the point.



(a) PSR state for  $\eta_0 = -0.9, \sigma = 0.8$  and  $\kappa = -2$ . The mean field settles onto a stable node.

(b) PSS state for  $\eta_0 = 0.5, \sigma = 0.7$  and  $\kappa = 2$ . The mean field settles onto a stable focus.

(c) CPW state for  $\eta_0 = 10.75, \sigma = 0.5$  and  $\kappa = -9$ . The mean field settles onto a stable limit cycle.

Figure 14: Three macroscopic states observed in the *MFR* inside the imaginary unit circle  $|Z(t)| = 1$ . Green arrows mark the phase space vector field and blue trails mark solution curves. Red points indicate equilibrium points, found by the fixed-point iteration. The dotted line in the *CPW* state is the limit cycle of the fixed-degree networks, added for reference

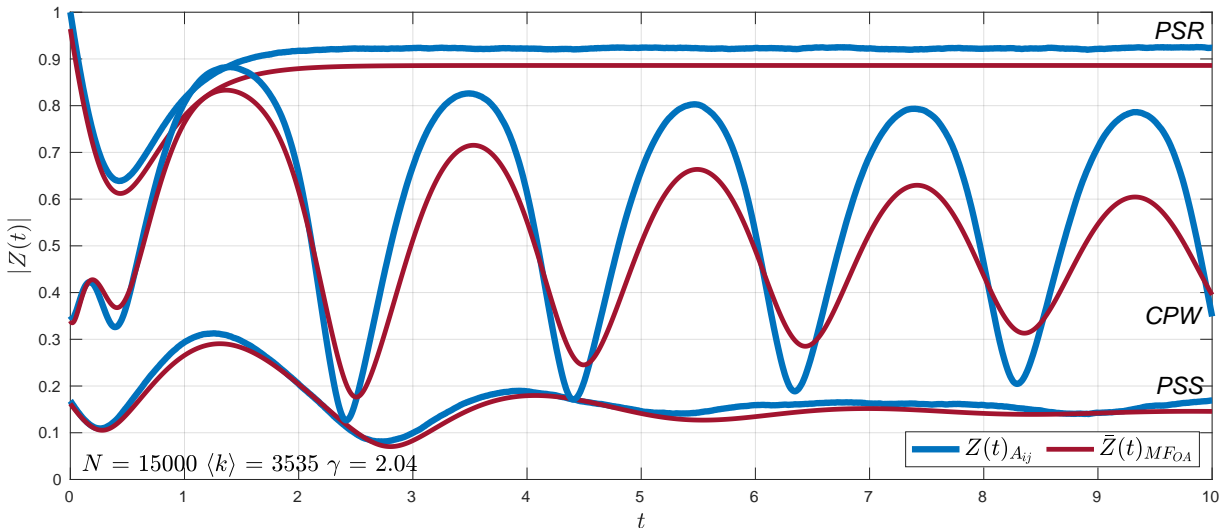


Figure 15: Comparison of the simulation of a scale-free network of Theta neurons and the Ott-Antonsen theory by the magnitude of the order parameter.

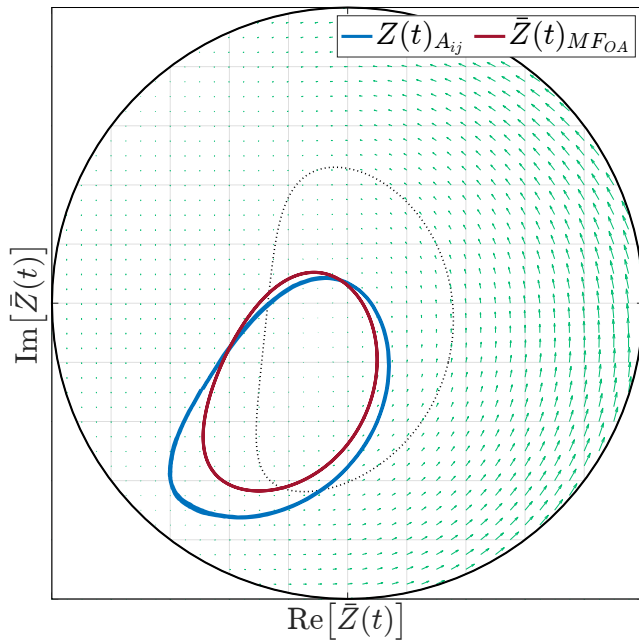


Figure 16: Comparison of the limit cycles found by theory and simulation.

## 7 Hebbian Learning and Synaptic Plasticity

*When an axon of cell A is near enough to excite a cell B and repeatedly or persistently takes part in firing it, some growth process or metabolic change takes place in one or both cells such that A's efficiency, as one of the cells firing B, is increased.* [11]

This quote from Hebb has influenced the neuroscientific community since 1949. In its essence, Hebb postulated that neurons that *fire together, wire together*. It has since become known as *Hebbian learning*, and is simply modelled as a positive correlation between the action potentials of spiking neurons. It has been proven *in vivo* in many studies [27], just like its counterpart, *anti-Hebbian learning*, where a negative correlation can be found.

### 7.1 Spike-timing dependant plasticity

One specific temporal interpretation of these ideas is *spike-timing-dependent plasticity (STDP)*, where the relative timing of action potentials from the pre- and postsynaptic neuron determine causality [28, 29]. If the postsynaptic neuron fires right after the presynaptic neuron, then we can expect the synaptic strength from post- to presynaptic neuron to increase, and vice versa.

Let us say that neuron  $\theta_i$  spikes at time  $t_i$  and that neuron  $\theta_j$  spikes at  $t_j$ . Taking the time difference  $\Delta t_{ij}$  as  $t_j - t_i$ , we can say that when  $\Delta t_{ij} > 0$  the spikes are correlated (there exists a temporally causal relation), and we can model an increase in synaptic strength of the connection from  $\theta_i$  to  $\theta_j$ , which we will gather in the *coupling matrix*  $K_{ij}$ . In the same fashion we can decrease  $K_{ji}$  when  $\Delta t_{ij} < 0$  as there is no causal relation.

We will find an expression for  $\Delta K_{ij}$  in function of  $\Delta t_{ij}$  so that at each time-step we can update  $K_{ij} \leftarrow K_{ij} + \Delta K_{ij}$ .

We can think of the coupling matrix as the continuous interpretation of  $\kappa A_{ij}$ , where synaptic strength and network topology go hand in hand. This also means that we need to redefine some concepts:

$$\mathbf{k}_i^{\text{in}} = \sum_{j=1}^N |K_{ij}| \quad \mathbf{k}_j^{\text{out}} = \sum_{i=1}^N |K_{ij}| \quad \langle k \rangle = \frac{1}{N} \sum_{i,j=1}^N |K_{ij}| \quad (36)$$

The absolute value ensures that we capture the magnitude of the coupling strength. The reason we want to distinguish between  $\langle k \rangle$  and  $\langle \hat{k} \rangle$  is that for some parts of the investigation it is beneficial to study how inhibitive and excitatory coupling strengths influence each other.

Also the network of Theta neurons needs a redefinition:

$$\dot{\theta}_i = (1 - \cos \theta_i) + (1 + \cos \theta_i) \cdot [\eta_i + I_i(t)] \quad \theta_i \in \mathbb{T}^N \quad (37)$$

$$I_i(t) = \frac{1}{\langle k \rangle} \sum_{j=1}^N K_{ij} \cdot \mathcal{P}_n(\theta_j) \quad (38)$$

The functions  $W(t)$  that relate  $\Delta t_{ij}$  to  $\Delta K_{ij}$  are called *learning windows*, as they define a range in which  $K_{ij}$  is able to adapt or *learn*, and also when learning is optimal. When signals between neurons show a very large time difference (negative or positive) we do not expect them to be correlated. Because the learning windows are generally not symmetrical we can also expect the coupling matrix to be asymmetrical. The magnitude of these functions is small, as it is assumed that learning dynamics happen at a slower timescale than the neuronal dynamics.

Another characteristic is the integral over the learning window. A window with a negative integral directs synaptic strengths mostly towards inhibitory behaviour, and vice versa with a positive integral. An integral of zero would mean that both inhibitory and excitatory synapses are stimulated equally. It has been proven that  $\int W(\tau) d\tau$  is the magnitude of the correlation between signals [29].

This approach simplifies modelling the neuronal back-propagation, where another pulse is generated as an echo of the action potential which travels through the neuron dendrites (so, backwards). This behaviour is believed to adjust the presynaptic weights, though it is a controversial subject [29].

## 7.2 Formulations of *STDP* as a model

### 7.2.1 The Kempter method

Analysis of a distinct *STDP* model was done in [28]. Following the notation, we will denote the sequence of action potentials, the *spike train*, coming from each neuron  $\theta_i$  as  $S_i^{\text{out}}(t) = \sum_n \delta(t - t_i^n)$ , where  $t_i^n$  is the time that  $\theta_i$  has fired. Similarly, we will denote the spike train coming into each neuron  $\theta_i$  as  $S_i^{\text{in}}(t) = \sum_f \delta(t - t_i^f)$  with  $t_i^f$  being the time that a neighbouring neuron has spiked. Now we can say that the synaptic strengths are adjusted as:

$$\Delta K_{ij} = \int_t^{t+\mathcal{T}} w^{\text{out}} S_i^{\text{out}}(\tau) + w^{\text{in}} S_j^{\text{in}}(\tau) d\tau + \iint_t^{t+\mathcal{T}} W(\tau' - \tau) S_i^{\text{out}}(\tau) S_j^{\text{in}}(\tau') d\tau d\tau' \quad (39)$$

$$= \sum_{t_i^n \in \mathcal{T}} w^{\text{out}} + \sum_{t_j^f \in \mathcal{T}} w^{\text{in}} + \sum_{t_j^f, t_i^n \in \mathcal{T}} W(t_j^f - t_i^n) \quad (40)$$

with  $\mathcal{T}$  the period over which learning occurs.  $w^{\text{in}} > 0$  and  $w^{\text{out}} < 0$  are small weights on the in- and outgoing action potentials. In (39) we can recognise the correlation between signals as a convolution over the learning window. We will refer to (40) as the Kempter method.

The following learning window is proposed:

$$W(t)_K = A \begin{cases} \left[ \left(1 - \frac{t}{\tilde{\tau}_p}\right) - \left(1 - \frac{t}{\tilde{\tau}_n}\right) \right] \cdot \exp\left(\frac{t}{\tau_{\text{syn}}}\right) & \text{for } t \leq 0 \\ \exp\left(-\frac{t}{\tau_p}\right) - \exp\left(-\frac{t}{\tau_n}\right) & \text{for } t > 0 \end{cases} \quad (41)$$

Here  $t$  is the delay between presynaptic spike arrival and postsynaptic firing,  $A$  is a small learning parameter and all  $\tau$  are time constants. The values are given as  $A = 10^{-5}$ ,  $\tau_{\text{syn}} = 5 \text{ ms}$ ,  $\tau_p = 1 \text{ ms}$  and  $\tau_n = 20 \text{ ms}$ .  $\tilde{\tau}_p \equiv \tau_{\text{syn}}\tau_p / (\tau_{\text{syn}} + \tau_p)$  and  $\tilde{\tau}_n \equiv \tau_{\text{syn}}\tau_n / (\tau_{\text{syn}} + \tau_n)$ .  $\int W(t)_K d\tau = 4.75 \times 10^{-8}$  so that the correlation is positive.

$w^{\text{in}}$  and  $w^{\text{out}}$  are necessary for  $K_{ij}$  to reach an equilibrium, which is proven from the average learning dynamics. Using an inhomogeneous Poisson process with time-dependent intensities to generate spike trains, the learning equation (40) is found to converge to a stable equilibrium, also when different types of noise are added to selections of neurons [28]. The authors do understand the concept of topology, as the variation of the coupling strength between nodes is examined, but they did not investigate the relation of coupling strength between nodes. The question will now be whether convergence of the synaptic strength still occurs when we will apply *STDP* to our network of Theta neurons, as changes to the coupling strength will also influence the spiking dynamics between neurons, which in turn will affect the learning again. The distribution of spikes in each spike train might not be coming from a recognisable distribution.

To counteract the excitatory nature of the learning window, the authors propose  $w^{\text{in}} = A$  and  $w^{\text{out}} = -1.0475 \cdot A$  so that the amplitude of these weights is on the same order as the magnitude

of the learning window [28]. This is a regulatory process, as neurons are punished for sending out many spikes over time by decreasing their influence over neighbours more than the increase in influence of their neighbours over them. This threshold can be overcome by teaching the neurons to spike at the right time (with respect to its neighbours' spikes) as then the learning window yields an increase in synaptic strength.

### 7.2.2 The Song method

Another formulation of *STDP* as a mathematical model can be found in [30]. It is postulated without being concerned about the biological aspect too much, simplifying some of the ideas of [28]. The synaptic strengths are simply updated with:

$$\Delta K_{ij} = K^{\max} \cdot \sum_{t_j^f, t_i^n \in \mathcal{T}} W(t_j^f - t_i^n) \quad (42)$$

where  $K^{\max}$  is the maximum allowed synaptic strength, so that we can think of (42) as taking a percentage of the maximum coupling. The authors also constrain  $0 \leq K_{ij} \leq K^{\max}$ , as there is no regulatory process like in (40). In their further work on *STDP* and *IP* the authors booked remarkable progress, and their work on the Izhikevich model is very interesting for our application [31]. We will refer to (42) as the Song method.

The learning window is then again defined as a discontinuous function:

$$W(t)_S = \begin{cases} A_n \cdot \exp\left(\frac{t}{\tau_n}\right) & \text{for } s \leq 0 \\ A_p \cdot \exp\left(\frac{-t}{\tau_p}\right) & \text{for } s > 0 \end{cases} \quad (43)$$

where we will use  $A_p = 0.005$ ,  $A_n = -0.00525$  and  $\tau_p = \tau_n = 20$  ms.  $\int W(\tau)_S d\tau = -5.0 \times 10^{-6}$  so we expect the weights to be suppressed towards a negative value. Interestingly, the line between reward and punishment is very thin, as the largest increase and largest decrease in synaptic strength lie right next to each other on the spectrum.

As  $K_{ij}$  is only allowed to be positive, the negative correlation of the learning window pushes most of the synaptic strengths towards zero. The range of coupling strengths is also very restricted and only allowed to change over a small interval:  $K^{\max} = 0.03$  [30–32]. The learning dynamics, encoded into the topology of the network, show how the node degrees are pushed towards the edges  $\pm K^{\max}$  with only a small group of neurons managing to learn the optimal spiking time. The spiking rate of all nodes in the network converges to a normal distribution. However, no mention is made of convergence of the node degrees, as the learning procedure is halted artificially.

Recently, triphasic learning windows have been used to account for when it takes too long for the postsynaptic neuron to fire, and thus to decorrelate the relation between neurons. These learning windows are curves that were fitted to experimental data of the cortex and the hippocampus [27]. Extending the work of [30] we can find a brief investigation of network topology and clustering using triphasic windows, [32]. The method is as in (43), with the following learning window:

$$W(t)_C = A_p \cdot \exp\left(\frac{-(t-15)^2}{\tau_p}\right) - A_n \cdot \exp\left(\frac{-(t-20)^2}{\tau_n}\right) \quad (44)$$

where  $A_p = 0.23$ ,  $A_n = 0.15$ ,  $\tau_p = 200$  and  $\tau_n = 2000$ .  $\int W(s)_C ds = -6.0 \times 10^{-3}$ .

When comparing the qualities of the different learning windows presented here, one can quickly notice the difference in magnitude between the learning windows. That does not necessarily include the magnitude of the correlation, but the magnitude of the window itself. In (41), the learning rate is a few orders of magnitude smaller than in (44) and this resulted in extremely slow convergence when testing. For (43) this issue was solved in [32] by using  $A_p = 0.1$  and  $A_n = -0.12$ . In the same spirit, we will therefore use  $A = 8.0 \times 10^{-2}$  in (41). These alterations yield  $\int W(\tau)_S d\tau = -4.0 \times 10^{-4}$  and  $\int W(\tau)_K d\tau = 3.8 \times 10^{-4}$ .

It is important to notice that learning only occurs when neurons spike, so that equilibrium states will disturb the learning process. However, these states were rarely encountered during the testing process, and it seems like there continues to exist enough randomness in the states of  $\theta_i$  to persist spiking. When implementing *STDP*, a time-step smaller than 0.01 is necessary, otherwise important details in the learning dynamics that are captured by the shape of the learning window will be lost. Another important observation is that when computing the time delay between spikes,  $t_i^f - t_i^n$  will always be zero by definition. It is much simpler to perform this operation than to filter it out. In the case that  $W(0)$  is zero,  $K_{ii}$  will not change. Though for  $W_S$  and  $W_C$  we have  $W(0) < 0$  so that  $K_{ii}$  will always be decrease in magnitude. Conclusions can therefore not be drawn from the diagonal of  $K$ .

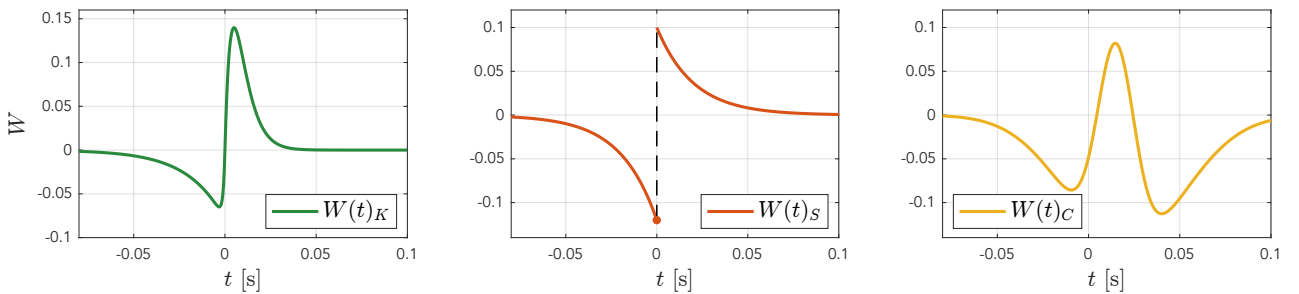


Figure 17: Three different biphasic learning windows. Left: with  $W_K$  the the learning spectrum is quite narrow. Middle: we can see how in  $W(t)_S$  a slightly larger emphasis is put on the anti-Hebbian learning. Right: a triphasic window can punish the synaptic strength when signals arrive either too early or too late.

In recent years, criticism on *STDP* has been growing, as experimental data has shown that *STDP* is usually accompanied by homeostatic plasticity of the neurons excitability and the synaptic strength. Basing our learning behaviour on the correlation between neuronal activity can be quite unstable: changes to the synaptic strength cause changes in the postsynaptic firing rate, which generates further changes to the synaptic strength in a positive feedback loop. Processes like *intrinsic plasticity (IP)*, where one neuron's excitability changes over time as to self-regulate sensitivity to incoming action potentials, or *synaptic scaling*, where synapse characteristics are adjusted in unison to counteract positive feedback loops, have proven to stabilise the synchronisation [27, 33]. When *STDP* and *IP* are combined, it seems like the two process balance each other out and stable network topologies can be found [31].

### 7.3 Synaptic scaling

There is no upper or lower bound on the synapse strength, and generally connection strengths are nonzero. Positive reinforcement loops might disturb the learning process, which would not be beneficial for the model. One technique we can apply to keep the strengths within a definitive range is to scale homeostatically - a method where any increases in synaptic strength will balance

out any decreases by scaling:

$$K_{ij}^s = K_{ij} \frac{\frac{1}{N} \sum_{i,j} K_{ij}}{\sum_i K_{ij}} \quad (45)$$

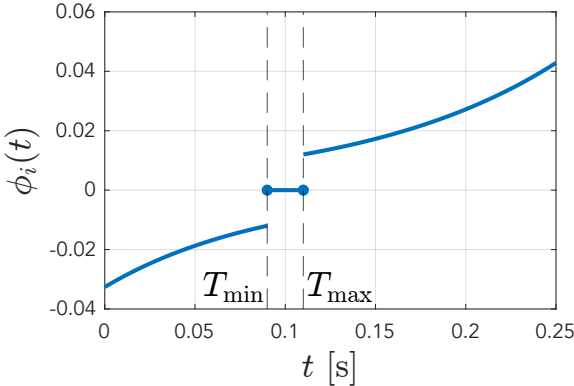
In this way, the out-degrees will remain constant. Using this approach, something has to remain constant, whether that is  $\langle k \rangle$ , or  $\langle k \rangle^2$  or any other property of the adjacency matrix. However, this property is not one we are after: we want a method that is able to change the network topology entirely.

## 7.4 Intrinsic plasticity

Instead of scaling the weights to preserve a certain quantity in the network, we can allow the neurons to adjust their sensitivity to incoming signals. So when some synaptic strengths are increased, we can reduce the excitability, and vice-versa. This should counteract positive feedback.

If we look at the formulation of the network of Theta neurons (38), we can see that  $\eta_i$  is the threshold on  $I_i(t)$  for which the result of the PRC will be positive or negative. The neuron action potentials  $\mathcal{P}_n(\theta_j)$  are scaled by the coupling matrix and the mean node degree. We expect that when neurons learn to adapt  $K_{ij}$  and  $\eta_i$ , the two will try to cancel each other out.

In [31] an *IP* method is introduced in detail. We can simply update  $\eta_i \leftarrow \eta_i + \eta_{\max} \cdot \phi_i$ , where:



$$\phi_i(t) = \begin{cases} -\alpha \cdot \exp\left(\frac{T_{\min}-t}{T_{\min}}\right) & t < T_{\min} \\ \alpha \cdot \exp\left(\frac{t-T_{\max}}{T_{\max}}\right) & t > T_{\max} \\ 0 & T_{\min} \leq t \leq T_{\max} \end{cases} \quad (46)$$

The argument  $t$  represents the time that has passed between successive spike of the same neuron, the *inter-spike interval (ISI)*. This is always a positive number.

The results of introducing *IP* seem to stabilise the resulting topologies in the Song method. Many more nodes seem to survive with a node degree that is not at the extremes, and there seems to exist an interesting relation between in- and out-degree vectors.

## 8 Investigation: Emerging Network Topologies

We will now investigate what topologies emerge from the learning procedures described in Chapter 7. Are the approaches presented in [28, 30–32] plausible within the context of the Theta model? Do we obtain similar results concerning synchronisation and topology? Is there a reason for only allowing the network to make excitatory ( $K_{ij} \geq 0$ ) connections?

### 8.1 Conditions of the network

As we saw in Chapter 5, the typical range for the coupling strength  $\kappa$  and the mean excitability  $\eta_0$  to alter the macroscopic state of the network drastically is fairly large. Using the Kempter method (40), there is no limit on the magnitude of  $K$ , though activity of the node degrees was observed within the interval [-100, 100].

When using the Song method (42) we will constrain  $-K^{\max} \leq K_{ij} \leq K^{\max}$  to allow neurons to both exhibit excitatory and inhibitory behaviour. When testing different values of  $K^{\max}$  no significant difference was observed in the results, except the time of reaching convergence of  $\langle k \rangle$ . To optimally compare the two methods we will use  $K^{\max} = 100$ .  $K_{ij}$  is initialised using a uniform distribution over  $[-K^{\max}, K^{\max}]$ , as to minimise influence of the initial distribution on the resulting topology.

The networks we will study consist of 100 Theta neurons, as the computational task of numerically solving the learning equations until convergence is a heavy one. Larger networks are more difficult to simulate, but smaller networks might be more susceptible to the stochastic behaviour of a few neurons. The networks will be initialised with  $\theta_i$  equidistantly distributed over  $\mathbb{T}$ , so that  $|Z(0)| = 0$  exactly. The excitabilities  $\eta_i$  are set to zero for all neurons. When investigating STDP + IP, the excitability is allowed to change over the same domain as  $K_{ij}$ , in accordance to our comments on  $\eta_i$  and  $I_i$  cancelling each other out. Therefore we take  $\eta_{\max} = K^{\max}$  and just like  $K_{ij}$ ,  $\eta_i$  is using a uniform distribution over  $[-\eta_{\max}, \eta_{\max}]$ .

### 8.2 Tuning hyperparameters for $W_K$

We decided to scale all learning windows presented in Chapter 7 to the same order of magnitude, to make for a fair comparison of the learning dynamics over time. What is left now is to tune the hyperparameters  $w^{\text{in}}$  and  $w^{\text{out}}$ . Looking at Figure 18, we can see that we cannot simply use the same magnitude as the learning window: the dynamics are disturbed by the large discrete changes induced by  $w^{\text{in}}$  and  $w^{\text{out}}$ . A better solution is obtained by using  $w^{\text{in}} = 10^{-3}$ .

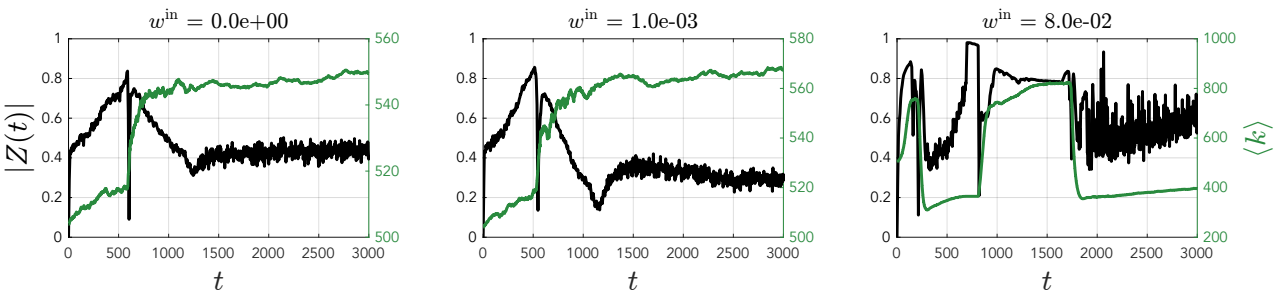


Figure 18: Tuning of the hyperparameters  $w^{\text{in}}$  and  $w^{\text{out}} = -1.0475 \cdot w^{\text{in}}$ . The radius of the order parameter is initialised as zero and quickly becomes non-zero. When neurons start bursting we can see a big drop in synchronisation, and a large increase in  $k$ , meaning that the STDP method works. Left: the learning dynamics with zero weights, as a benchmark. Middle: the learning dynamics for small, non-zero weights. The mean coupling strength is higher, but the overall synchronisation is lower. This might yield an interesting topological structure. Right: the learning dynamics with the same magnitude as the learning window disturb the learning process.

### 8.3 Results of using *STDP*

We can now use the Kempter method and its corresponding learning window and compare it to the Song method and the bi- and triphasic learning windows. The results are shown in Figure 19. It is remarkable how easily the different methods can be recognised, not to speak of the influence of the magnitude of the correlation, which using  $W_C$  shows the most amount of learning. Interestingly, the networks show a high degree of symmetry.

In the first column of plots, we can see the overall synchronisation of the network and its mean node degree as it learns over time. The Kempter method does not seem to converge for any time period under the circumstances described before. We find the network right before larger node degrees start taking off to higher orders, and remarkably the synchronisation is very low. The coupling matrix does not seem to contain a lot of structure until we look at the histogram underneath: a lognormal shape can be identified. Remember that no constraints are applied to  $K$ , so its is remarkable a structure seems to appear. Looking at the distributions of the in- and out-degrees, we can see they follow a positive correlation, with a more clustered behaviour for high degrees.

In the second column we can see the results of using the Song method with  $W_S$ . The learning behaviour is more regular and we can observe that with an increasing network connectivity we obtain increased synchronisation. Convergence is near completion, and we can see the separation between two clusters of node degrees in the high-contrast image of  $K$ , and in all histograms and plots. We can interpret the scatterplot of  $k^{\text{in}}$  versus  $k^{\text{out}}$  as a small group of nodes of varying degrees, and a large group of node degrees at the limits, as the definition of the degree vectors (36) takes only the absolute value. Most neurons see their synaptic strength decreased by the negative correlation. There is only a small fraction of oscillators that has learned to spike at the right time and manages to keep increasing its synaptic strength and eventually ends up at  $K^{\max}$ .

In the third column we can see the results of using the Song method with  $W_C$ . Convergence to a steady-state happens much more steadily, and also the synchronisation benefits from this approach. The coupling matrix shows an even stronger partition, as even fewer neurons manage to learn to spike at the right interval.

It is useful to review our choice to define  $k^{\text{in}}$  from the absolute value of  $K_{ij}$ . One can see this operation as folding the histogram of  $K$  in half at 0, and argue that inherently information is lost. However, when not accounting for the sign of the synaptic strength, they might cancel out and a node degree of zero might be found for even the best connected neurons. What we do lose is the ability to see positive or negative correlation, but that information can be found from the learning window, or from the mean value of the histogram of  $K$ .

### 8.4 Results of using *STDP + IP*

When introducing intrinsic plasticity, the expected changes to  $\eta_i$  counteract  $K$  as expected:  $\eta_i$  is cranked up to the largest possible value for virtually all neurons, but it seems to have an effect. The results are shown in Figure 20.

We find the Kempter method again on the verge of exploding, where nodes with a large degree (both negative and positive) are about to take off to even larger orders of magnitude. The overall structure is similar as before, but the positive correlation between in- and out-degrees is stronger. The Song method benefits from a faster convergence, which we can see in the second and third column. This is likely due to the neurons becoming less susceptible with an increased excitability. A more uniform distribution of node degrees can be found between the two extrema, as convergence has halted. For both methods the dichotomy between low and high degree nodes is more clear,

especially for  $W_C$ .

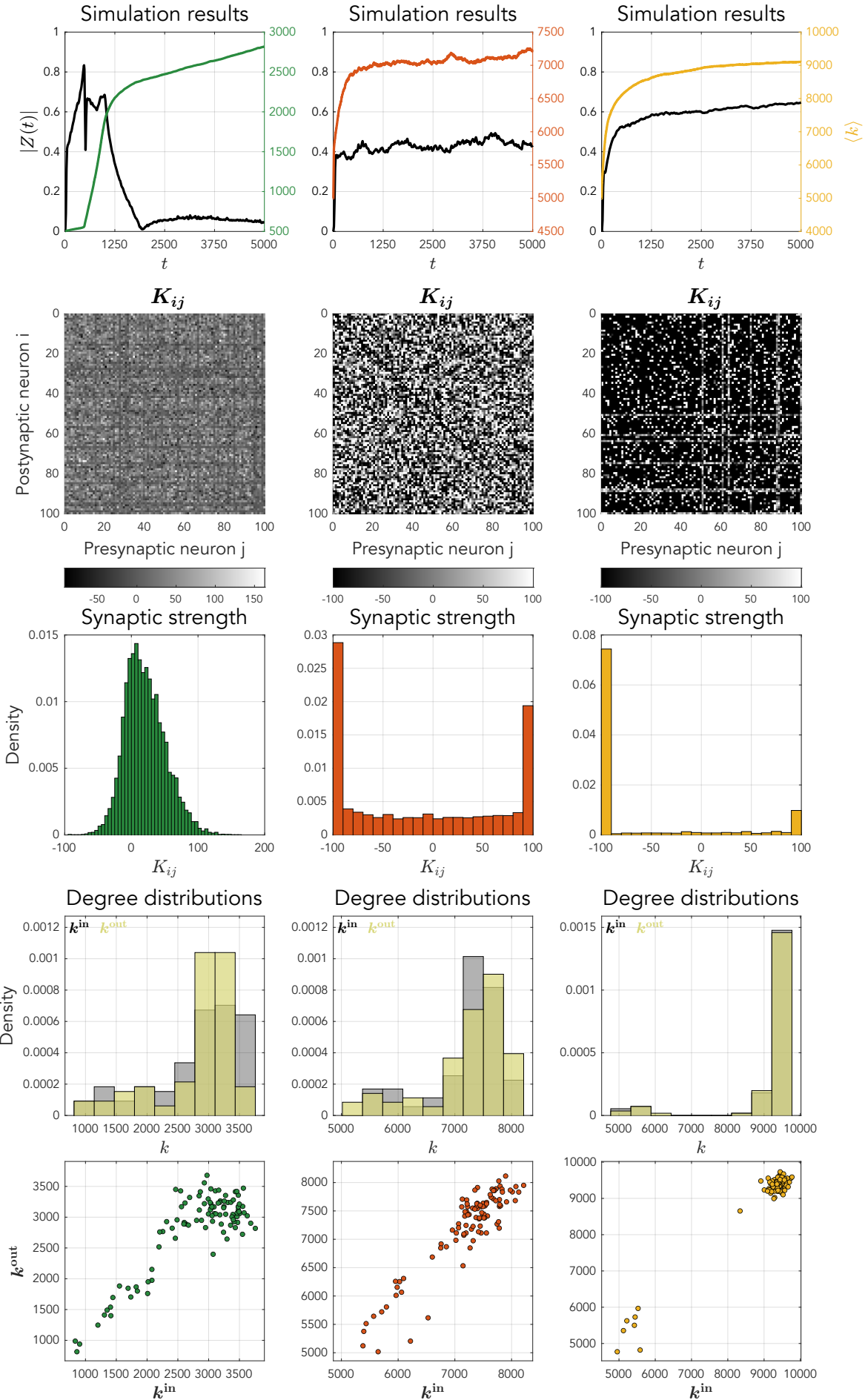


Figure 19: Results of the STDP learning.

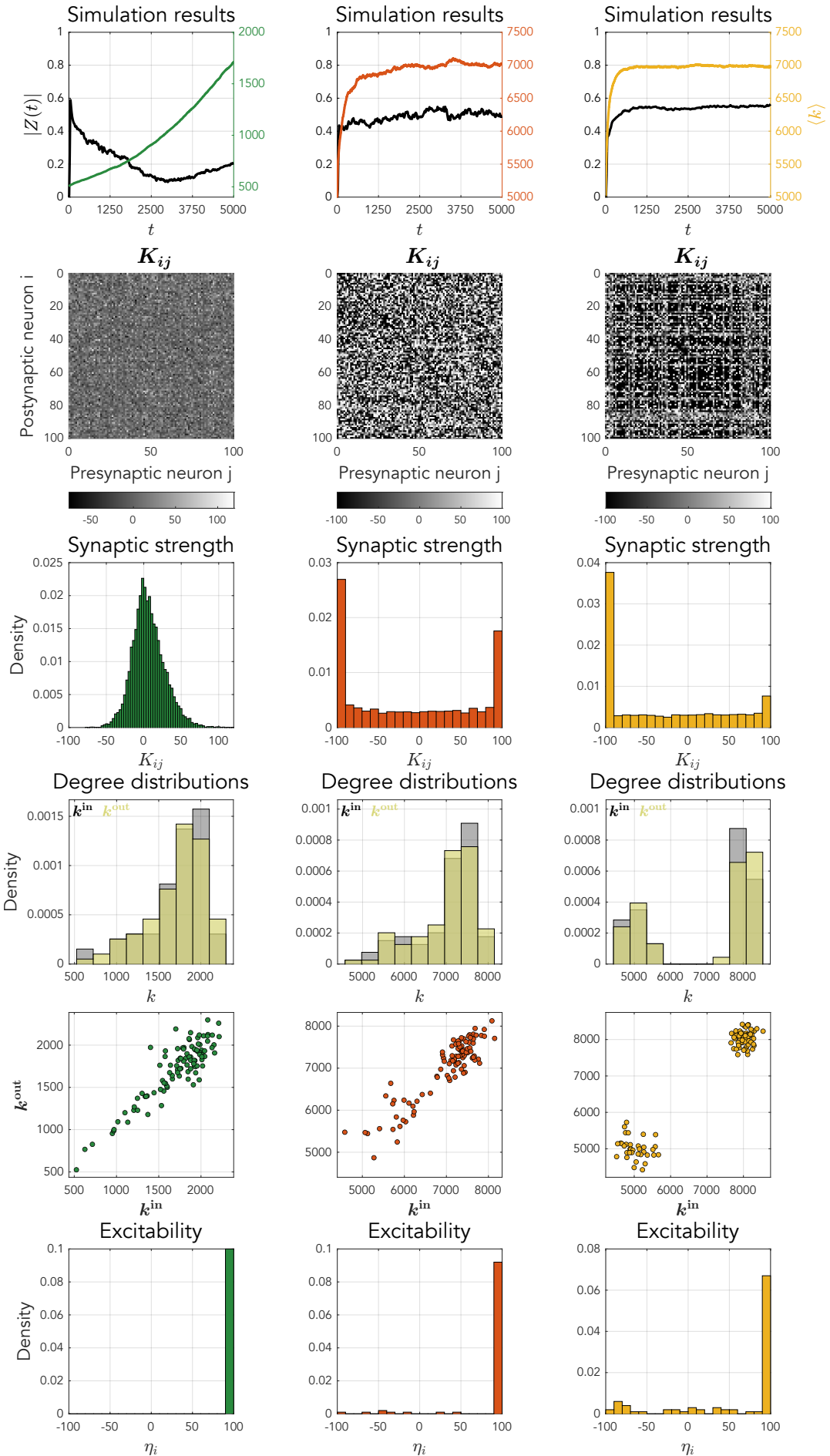


Figure 20: Results of the STDP learning with IP learning.

## 9 Conclusion and Discussion

**TODO:** *what did we achieve with this work?*

## 10 References

- [1] Human Brain Project, 2017. <https://www.humanbrainproject.eu/en/>. Accessed: 28.05.2020.
- [2] C. Börgers, *An Introduction to Modeling Neuronal Dynamics*. Texts in Applied Mathematics. Springer International Publishing, 2018.
- [3] The Nobel Prize in Physiology or Medicine 1963, 2009. <https://www.nobelprize.org/prizes/medicine/1963/speedread/>. Accessed: 28.05.2020.
- [4] S. Herculano-Houzel, *The Human Brain in Numbers: A Linearly Scaled-up Primate Brain*. *Frontiers in human neuroscience* **3** (11, 2009) 31.
- [5] E. Bullmore and D. Bassett, *Brain Graphs: Graphical Models of the Human Brain Connectome*. *Annual review of clinical psychology* **7** (04, 2010) 113–40.
- [6] E. Ott and T. M. Antonsen, *Low Dimensional Behavior of Large Systems of Globally Coupled Oscillators*. [arXiv:0806.0004 \[nlin.CD\]](https://arxiv.org/abs/0806.0004).
- [7] S. Chandra, D. Hathcock, K. Crain, T. Antonsen, M. Girvan, and E. Ott, *Modeling the Network Dynamics of Pulse-Coupled Neurons*. *Chaos (Woodbury, N.Y.)* **27** (03, 2017) 10.
- [8] The University Of Queensland Brain Institute, *Action potentials and synapses*. <https://qbi.uq.edu.au/brain-basics/brain/brain-physiology/action-potentials-and-synapses>. Composed: 09/11/2017. Accessed: 02/10/2020.
- [9] B. Ermentrout and D. Terman, *The Mathematical Foundations of Neuroscience*. vol. Vol. 35. Springer, July, 2010.
- [10] X. Zhang and J. Feng, *Computational modeling of neuronal networks*. [arXiv:1203.0868 \[q-bio.NC\]](https://arxiv.org/abs/1203.0868).
- [11] D. O. Hebb, *The organization of behaviour: a neurophysical theory*. John Wiley and sons, 1949.
- [12] F. C. Hoppensteadt and E. M. Izhikevich, *Canonical Neural Models*., 2001.
- [13] A. Hodgkin, *The local electric changes associated with repetitive action in a non-medullated axon*. *The Journal of physiology* **107** no. 2, (March, 1948) 165—181. <https://www.ncbi.nlm.nih.gov/pmc/articles/pmid/16991796/?tool=EBI>.
- [14] B. Ermentrout and N. Kopell, *Parabolic Bursting in an Excitable System Coupled with a Slow Oscillation*. *Siam Journal on Applied Mathematics - SIAMAM* **46** (04, 1986) 233–253.
- [15] T. Luke, E. Barreto, and P. So, *Complete Classification of the Macroscopic Behavior of a Heterogeneous Network of Theta Neurons*. *Neural Computation* **25** (12, 2013) 1–28.
- [16] B. Gutkin, *Theta-Neuron Model*. Springer New York, New York, NY, 2013. [https://doi.org/10.1007/978-1-4614-7320-6\\_153-1](https://doi.org/10.1007/978-1-4614-7320-6_153-1).
- [17] F. A. Pérez, *Phase-responsiveness transmission in a network of quadratic integrate-and-fire neurons*. Universitat Politècnica de Catalunya, Facultat de Matemàtiques i Estadística (January, 2020) . Bachelor Thesis.
- [18] B. Ermentrout, *Type i Membranes, Phase Resetting Curves, and Synchrony* *Neural Comput.* **8** no. 5, (July, 1996) 979–1001. <https://doi.org/10.1162/neco.1996.8.5.979>.
- [19] P. Erdos and A. Rényi, *On Random Graphs I*. *Publicationes Mathematicae* **6** (1959) 290–297.
- [20] A. Barabási, *Network Science*. Cambridge University Press, 2016. <https://books.google.dk/books?id=iLtGDQAAQBAJ>.

- [21] A.-L. Barabási and E. Bonabeau, *Scale-Free Networks*. *Scientific American* **288** no. 60-69, (2003) 50–59. <http://www.nd.edu/~networks/PDF/Scale-Free%20Sci%20Amer%20May03.pdf>.
- [22] C. I. Del Genio, T. Gross, and K. E. Bassler, *All Scale-Free Networks Are Sparse*. *Phys. Rev. Lett.* **107** (Oct, 2011) 178701. <https://link.aps.org/doi/10.1103/PhysRevLett.107.178701>.
- [23] C. Bick, M. Goodfellow, C. Laing, and E. Martens, *Understanding the dynamics of biological and neural oscillator networks through exact mean-field reductions: a review*. *Journal of Mathematical Neuroscience* **10** no. 1, (Dec., 2020) .
- [24] E. Ott and T. M. Antonsen, *Long Time Evolution of Phase Oscillator Systems*. [arXiv:0902.2773 \[nlin.CD\]](https://arxiv.org/abs/0902.2773).
- [25] E. Ott, B. R. Hunt, and T. M. Antonsen, *Comment on "Long Time Evolution of Phase Oscillator Systems"* [*Chaos* 19, 023117 (2009), arXiv: 0902.2773]. [arXiv:1005.3319 \[nlin.CD\]](https://arxiv.org/abs/1005.3319).
- [26] J. Restrepo and E. Ott, *Mean field theory of assortative networks of phase oscillators* *EPL (Europhysics Letters)* **107** (07, 2014) .
- [27] J. Chrol-Cannon and Y. Jin, *Computational Modeling of Neural Plasticity for Self-Organization of Neural Networks*. *Bio Systems* **125** (04, 2014) .
- [28] R. Kempter, W. Gerstner, and L. van Hemmen, *Hebbian learning and spiking neurons*. *Phys. Rev. E* **59** (04, 1999) .
- [29] W. Gerstner and W. Kistler, *Mathematical Formulations of Hebbian Learning*. *Biological cybernetics* **87** (01, 2003) 404–15.
- [30] S. Song, K. Miller, and L. Abbott, *Competitive Hebbian learning through spike timing-dependent plasticity* *Nature neuroscience* **3** (10, 2000) 919–26.
- [31] X. Li, W. Wang, F. Xue, and Y. Song, *Computational modeling of spiking neural network with learning rules from STDP and intrinsic plasticity*. *Physica A-statistical Mechanics and Its Applications* **491** (2018) 716–728.
- [32] J. Chrol-Cannon, A. Grüning, and Y. Jin, *The emergence of polychronous groups under varying input patterns, plasticity rules and network connectivities* in *The 2012 International Joint Conference on Neural Networks (IJCNN)*, pp. 1–6, IEEE. 2012.
- [33] H. Lee and A. Kirkwood, *Mechanisms of Homeostatic Synaptic Plasticity in vivo*. *Frontiers in Cellular Neuroscience* **13** (Dec., 2019) .

## A Appendix

### A.1 Transformation to the QIF model

We prove that the transformation (2) holds from the QIF model (3) to the Theta model (1).

$$V \equiv \tan\left(\frac{\theta}{2}\right) \quad \rightarrow \quad \frac{dV}{dt} = \frac{1}{2 \cos^2\left(\frac{\theta}{2}\right)} \frac{d\theta}{dt}$$

Insert into  $\frac{dV}{dt} = V^2 + I$ :

$$\frac{d\theta}{dt} = 2 \left( \cos^2\left(\frac{\theta}{2}\right) \cdot \tan^2\left(\frac{\theta}{2}\right) + \cos^2\left(\frac{\theta}{2}\right) \cdot I \right) = 2 \left( \sin^2\left(\frac{\theta}{2}\right) + \cos^2\left(\frac{\theta}{2}\right) \cdot I \right)$$

Using  $\cos^2\left(\frac{\theta}{2}\right) = \frac{1+\cos(\theta)}{2}$  and  $\sin^2\left(\frac{\theta}{2}\right) = \frac{1-\cos(\theta)}{2}$ :

$$\dot{\theta} = 2 \left( \frac{1 - \cos \theta}{2} + \left( \frac{1 + \cos \theta}{2} \right) \cdot I \right) = (1 - \cos \theta) + (1 + \cos \theta) \cdot I$$

This proves that the transformation (2) is correct.

### A.2 Solutions to the QIF model

Depending on the value of  $I$ , we can distinguish multiple solutions [17]. In all cases we can integrate through the separation of variables. Solutions are bound to start at  $V(t_0)$ , right after a spike has occurred at  $t = t_0$ .

#### A.2.1 Solving for $I < 0$

$$\begin{aligned} \int_{V(t_0)}^{V(t)} \frac{dv}{v^2 - \tilde{I}^2} &= \int_{V(t_0)}^{V(t)} \frac{dv}{(v + \tilde{I})(v - \tilde{I})} = \frac{1}{2\tilde{I}} \int_{V(t_0)}^{V(t)} \frac{dv}{v - \tilde{I}} - \frac{1}{2\tilde{I}} \int_{V(t_0)}^{V(t)} \frac{dv}{v + \tilde{I}} \\ &= \frac{1}{2\tilde{I}} \log\left(1 - \frac{2\tilde{I}}{v + \tilde{I}}\right) \Big|_{V(t_0)}^{V(t)} = \int_{t_0}^t d\tau = t - t_0 \\ V(t) &= \lim_{V(t_0) \rightarrow -\infty} \frac{2\sqrt{-I}}{1 - \left(1 - \frac{2\sqrt{-I}}{V(t_0) + \sqrt{-I}}\right) \cdot e^{2(t-t_0)\sqrt{-I}}} - \sqrt{-I} \\ &= \frac{2\sqrt{-I}}{1 - e^{2(t-t_0)\sqrt{-I}}} - \sqrt{-I} \end{aligned}$$

#### A.2.2 Solving for $I = 0$

$$\begin{aligned} \int_{V(t_0)}^{V(t)} \frac{dv}{v^2} &= \frac{1}{v} \Big|_{V(t_0)}^{V(t)} = -\frac{1}{V(t)} + \frac{1}{V(t_0)} = \int_{t_0}^t d\tau = t - t_0 \\ V(t) &= \lim_{V(t_0) \rightarrow -\infty} \frac{V(t_0)}{1 - V(t_0)(t - t_0)} \stackrel{\text{H}}{\underset{\infty}{\approx}} \frac{-1}{t - t_0} \end{aligned}$$

#### A.2.3 Solving for $I > 0$

$$\begin{aligned} \int_{V(t_0)}^{V(t)} \frac{dv}{v^2 + I} &= \int_{V(t_0)}^{V(t)} \frac{I}{\left(\frac{v}{\sqrt{I}}\right)^2 + 1} dv \stackrel{x=\frac{v}{\sqrt{I}}}{=} \int_{\frac{V(t_0)}{\sqrt{I}}}^{\frac{V(t)}{\sqrt{I}}} \frac{I}{x^2 + 1} dx = \frac{1}{\sqrt{I}} \arctan(x) \Big|_{\frac{V(t_0)}{\sqrt{I}}}^{\frac{V(t)}{\sqrt{I}}} \\ &= \frac{1}{\sqrt{I}} \left( \arctan\left(\frac{V(t)}{\sqrt{I}}\right) - \arctan\left(\frac{V(t_0)}{\sqrt{I}}\right) \right) = \int_{t_0}^t d\tau = t - t_0 \\ V(t) &= \lim_{V(t_0) \rightarrow -\infty} \sqrt{I} \cdot \tan\left((t - t_0)\sqrt{I} + \arctan\left(\frac{V(t_0)}{\sqrt{I}}\right)\right) = \sqrt{I} \cdot \tan\left((t - t_0)\sqrt{I} - \frac{\pi}{2}\right) \\ &= \sqrt{I} \cdot \cot\left((t - t_0)\sqrt{I}\right) \end{aligned}$$

### A.3 Frequency response of the neuron models

The integral is solved like before, but now with the conditions of the spike:

$$\begin{aligned} T &= \lim_{a \rightarrow \infty} \int_{-a}^a \frac{I}{\left(\frac{v}{\sqrt{I}}\right)^2 + 1} dv \stackrel{x = \frac{v}{\sqrt{I}}}{=} \lim_{a \rightarrow \infty} \int_{\frac{-a}{\sqrt{I}}}^{\frac{a}{\sqrt{I}}} \frac{I}{x^2 + 1} dx = \lim_{a \rightarrow \infty} \frac{1}{\sqrt{I}} \arctan(x) \Big|_{\frac{-a}{\sqrt{I}}}^{\frac{a}{\sqrt{I}}} \\ &= \frac{1}{\sqrt{I}} \left( \frac{\pi}{2} - \left( -\frac{\pi}{2} \right) \right) = \frac{\pi}{\sqrt{I}} \end{aligned}$$

So the frequency of oscillation is proportional to  $\sqrt{I}$ .

### A.4 Newton-Raphson root iteration

We define the equilibria  $\mathbf{x}^* \in \mathbb{R}^n$  of a multivariate function  $\mathbf{f}(\mathbf{x}) : \mathbb{R}^n \rightarrow \mathbb{R}^n$  with  $\mathbf{f}(\mathbf{x}) = \mathbf{0}$ . Expanding  $\mathbf{f}$  as a Taylor series, we obtain:

$$f_i(\mathbf{x} + \delta\mathbf{x}) = f_i(\mathbf{x}) + \sum_{j=1}^n \frac{\partial f_i(\mathbf{x})}{\partial x_j} \delta x_j + O(\delta\mathbf{x}^2) \approx f_i(\mathbf{x}) + \sum_{j=1}^n \frac{\partial f_i(\mathbf{x})}{\partial x_j} \delta x_j, \quad (i = 1, \dots, n)$$

We can also write this in vector notation, by setting  $\mathbf{J}(\mathbf{x}) = \nabla \mathbf{f}(\mathbf{x}) = \frac{d}{d\mathbf{x}} \mathbf{f}(\mathbf{x}) \in \mathbb{R}^{n \times n}$

$$\mathbf{f}(\mathbf{x} + \delta\mathbf{x}) \approx \begin{bmatrix} f_1(\mathbf{x}) \\ \vdots \\ f_N(\mathbf{x}) \end{bmatrix} + \begin{bmatrix} \frac{\partial f_1}{\partial x_1} & \cdots & \frac{\partial f_1}{\partial x_N} \\ \vdots & \ddots & \vdots \\ \frac{\partial f_N}{\partial x_1} & \cdots & \frac{\partial f_N}{\partial x_N} \end{bmatrix} \begin{bmatrix} \delta x_1 \\ \vdots \\ \delta x_N \end{bmatrix} = \mathbf{f}(\mathbf{x}) + \mathbf{J}(\mathbf{x}) \delta\mathbf{x}$$

By assuming  $\mathbf{f}(\mathbf{x} + \delta\mathbf{x}) = \mathbf{0}$  we can find that  $\delta\mathbf{x} = -\mathbf{J}^{-1}(\mathbf{x})\mathbf{f}(\mathbf{x})$  so that  $\mathbf{x} + \delta\mathbf{x} = \mathbf{x} - \mathbf{J}^{-1}(\mathbf{x})\mathbf{f}(\mathbf{x})$ . This expression converges to  $\mathbf{x}^*$ . When the equations are nonlinear, the equations converge to the real root as  $\mathbf{x}_k = \mathbf{x}_k - \mathbf{J}^{-1}(\mathbf{x}_k)\mathbf{f}(\mathbf{x}_k)$ .

### A.5 Jacobian of the Ott-Antonsen manifold

Starting from (25), we separate the real and imaginary parts of  $z(\mathbf{k}, t)$  in  $x_{\mathbf{k}} = x(\mathbf{k}, t)$  and  $y_{\mathbf{k}} = y(\mathbf{k}, t)$ :

$$\begin{aligned} \frac{\partial z_{\mathbf{k}}}{\partial t} &= -\frac{i}{2} \cdot (x_{\mathbf{k}}^2 + i2x_{\mathbf{k}}y_{\mathbf{k}} - y_{\mathbf{k}}^2 - 2x_{\mathbf{k}} - i2y_{\mathbf{k}} + 1) + \frac{1}{2} \cdot (x_{\mathbf{k}}^2 + i2x_{\mathbf{k}}y_{\mathbf{k}} - y_{\mathbf{k}}^2 + 2x_{\mathbf{k}} + i2y_{\mathbf{k}} + 1) \cdot I_{\mathbf{k}} \\ I_{\mathbf{k}} &= -\sigma_{\mathbf{k}} + i\eta_{0,\mathbf{k}} + iH_{2\mathbf{k}} \\ H_{2\mathbf{k}} &= \frac{\kappa}{\langle k \rangle} \sum_{\mathbf{k}' \in \mathbb{K}} P(\mathbf{k}') a(\mathbf{k}' \rightarrow \mathbf{k}) \cdot \left( 1 + \frac{x_{\mathbf{k}}^2}{3} - \frac{4}{3}x_{\mathbf{k}} \right) \end{aligned}$$

Taking the dynamics per real and imaginary value yields:

$$\begin{aligned} \frac{\partial x_{\mathbf{k}}}{\partial t} &= f_{\mathbf{k}}(x_{\mathbf{k}}, y_{\mathbf{k}}) \\ &= (x_{\mathbf{k}} - 1)y_{\mathbf{k}} - \frac{(x_{\mathbf{k}} + 1)^2 - y_{\mathbf{k}}^2}{2}\sigma_{\mathbf{k}} + (x_{\mathbf{k}} + 1)y_{\mathbf{k}}[\eta_0 + H_{2\mathbf{k}}] \\ \frac{\partial x_{\mathbf{k}}}{\partial t} &= g_{\mathbf{k}}(y_{\mathbf{k}}, y_{\mathbf{k}}) \\ &= -\frac{(x_{\mathbf{k}} - 1)^2 - y_{\mathbf{k}}^2}{2} - (x_{\mathbf{k}} + 1)y_{\mathbf{k}}\sigma_{\mathbf{k}} + \frac{(x_{\mathbf{k}} + 1)^2 - y_{\mathbf{k}}^2}{2} \cdot [\eta_0 + H_{2\mathbf{k}}] \end{aligned}$$

And the Jacobian is found from the partial derivatives of  $f$  and  $g$ :

$$\begin{aligned}
\frac{\partial f_{\mathbf{k}}}{\partial x_{\mathbf{k}}} &= y_{\mathbf{k}} - (x_{\mathbf{k}} + 1)\sigma_{\mathbf{k}} - y_{\mathbf{k}}[\eta_0 + \kappa \cdot H_{2\mathbf{k}}] + (x_{\mathbf{k}} + 1)y_{\mathbf{k}} \frac{\partial H_{2\mathbf{k}}}{\partial x_{\mathbf{k}}} \\
\frac{\partial f_{\mathbf{k}}}{\partial y_{\mathbf{k}}} &= (x_{\mathbf{k}} - 1) + y_{\mathbf{k}}\sigma_{\mathbf{k}} + (x_{\mathbf{k}} + 1)[\eta_0 + H_{2\mathbf{k}}] \\
\frac{\partial g_{\mathbf{k}}}{\partial x_{\mathbf{k}}} &= -(x_{\mathbf{k}} - 1) - y_{\mathbf{k}}\sigma_{\mathbf{k}} + (x_{\mathbf{k}} + 1)[\eta_0 + H_{2\mathbf{k}}] + \left( \frac{(x_{\mathbf{k}} + 1)^2 - y_{\mathbf{k}}^2}{2} \right) \frac{\partial H_{2\mathbf{k}}}{\partial x_{\mathbf{k}}} \\
\frac{\partial g_{\mathbf{k}}}{\partial y_{\mathbf{k}}} &= y_{\mathbf{k}} - (x_{\mathbf{k}} + 1)\sigma_{\mathbf{k}} - y_{\mathbf{k}}[\eta_0 + H_{2\mathbf{k}}] \\
\frac{\partial H_{2\mathbf{k}}}{\partial x_{\mathbf{k}}} &= \frac{\kappa}{\langle k \rangle} P(\mathbf{k}) a(\mathbf{k} \rightarrow \mathbf{k})(x_{\mathbf{k}} - 2) \frac{2}{3} \\
\frac{\partial H_{2\mathbf{k}}}{\partial y_{\mathbf{k}}} &= 0
\end{aligned}$$

And the off-diagonal elements, the nodes represented by degree  $\mathbf{k}'$ :

$$\begin{aligned}
\frac{\partial f_{\mathbf{k}}}{\partial x_{\mathbf{k}'}} &= (x_{\mathbf{k}} + 1)y_{\mathbf{k}} \frac{\partial H_{2\mathbf{k}}}{\partial x_{\mathbf{k}'}} \\
\frac{\partial f_{\mathbf{k}}}{\partial y_{\mathbf{k}'}} &= 0 \\
\frac{\partial g_{\mathbf{k}}}{\partial x_{\mathbf{k}'}} &= \left( \frac{(x_{\mathbf{k}} + 1)^2 - y_{\mathbf{k}}^2}{2} \right) \frac{\partial H_{2\mathbf{k}}}{\partial x_{\mathbf{k}'}} \\
\frac{\partial g_{\mathbf{k}}}{\partial y_{\mathbf{k}'}} &= 0 \\
\frac{\partial H_{2\mathbf{k}}}{\partial x_{\mathbf{k}'}} &= \frac{\kappa}{\langle k \rangle} P(\mathbf{k}') a(\mathbf{k}' \rightarrow \mathbf{k})(x_{\mathbf{k}'} - 2) \frac{2}{3} \\
\frac{\partial H_{2\mathbf{k}}}{\partial y_{\mathbf{k}'}} &= 0
\end{aligned}$$